Quantum Sensing and Communication via Non-Gaussian States

Andrea Giani, *Student Member, IEEE*, Moe Z. Win, *Fellow, IEEE*, and Andrea Conti, *Fellow, IEEE*

***Abstract*—Quantum sensing and communication (QSC) is pivotal for developing next-generation networks with unprecedented performance. Many implementations of existing QSC systems employ Gaussian states as they can be easily realized using current technologies. However, Gaussian states lack non-classical properties necessary to unleash the full potential of QSC. This motivates the use of non-Gaussian states, which have non-classical properties beneficial for QSC. This paper establishes a theoretical foundation for QSC employing photon-varied Gaussian states (PVGSs). The PVGSs are non-Gaussian states that can be generated from Gaussian states using current technologies. First, we derive a closed-form expression for the generalized bilinear generating function of ordinary Hermite polynomials and show how it can be used to describe PVGSs. Then, we characterize PVGSs by deriving their Fock representation and their inner product. We also determine equivalence conditions for Gaussian states obtained from arbitrary permutations of rotation, displacement, and squeezing operators. Finally, we explore the use of PVGSs for QSC in several case studies.**

***Index Terms*—Quantum sensing, quantum communication, quantum information, non-Gaussian quantum states, quantum state characterization.**

I. Introduction

QUANTUM sensing and communication (QSC) is a promising field that has the potential to revolutionize information technologies, thus paving the way for the development of next-generation networks with unprecedented performance. Specifically, QSC underpins the extension of classical information theory fields, such as coding [1], [2], [3], [4], [5], [6], rate distortion [7], [8], [9], [10], [11], [12], sensing [13], [14], [15], and communication [16], [17], [18], [19] to the quantum domain. Quantum information technologies exploit properties of quantum mechanics to measure physical quantities of target systems and to exchange information. Such tasks are respectively referred to as quantum sensing [20], [21], [22], [23], [24], [25], [26], [27] and quantum communication [28], [29], [30], [31], [32], [33], [34], [35], [36], [37], [38], [39], [40], [41], [42], [43], [44], [45], [46], [47], [48], [49], [50], [51]. Many existing QSC systems are implemented with light sources that generate Gaussian quantum states. The use of Gaussian states is motivated by well-established theoretical foundations [52], [53], [54], [55], [56] and by the possibility of generating and manipulating them using current technologies. Unfortunately, Gaussian states do not possess several non-classical properties, including strong non-Poissonian photon number distribution and negative Wigner function [55], [56], [57], [58], [59], [60], [61], [62], which are necessary to fully unleash the potential of QSC. This calls for the use of non-Gaussian states, which play an important role toward achieving quantum supremacy [59], [60], [61]. However, the development of QSC systems employing non-Gaussian states can be challenging as it requires the implementation of complex optical processes, the characterization of such non-Gaussian states, and the establishment of theoretical foundations for QSC.

Non-Gaussian states are a broad class of quantum states that exhibit non-Gaussian Wigner function [61]. In the class of non-Gaussian states, photon-added quantum states (PAQSs) [63], [64], [65], [66] and photon-subtracted quantum states (PSQSs) [67], [68], [69], [70], [71] are of interest as they can be realized in laboratory [72], [73], [74], [75], [76], [77], [78] and their non-classical properties can be measured [78], [79], [80], [81], [82], [83]. In particular, PAQSs and PSQSs are obtained, respectively, by exciting and annihilating photons from an initial state of the quantized electromagnetic field. Recently, PAQSs and PSQSs have been unified in terms of photon-varied quantum states (PVQSs), which are obtained via photon-variation operations on initial quantum states [84]; such a photon-variation unifies photon-addition and photon-subtraction. When photon-variation operations are performed on initial Gaussian states, the corresponding PVQSs are referred to as photon-varied Gaussian states (PVGSs). An important property of PVGSs is their generality, as they reduce to Gaussian states under certain conditions. In the literature, subclasses of PVGSs have been used for quantum sensing [85], [86], [87], [88], [89], [90] and quantum communications [91], [92], [93], [94], [95], [96], [97], [98], showing that their degrees of freedom can be engineered to provide performance improvements compared to Gaussian states.

Received 15 November 2023; revised 13 May 2024 and 23 September 2024; accepted 25 October 2024. Date of publication 11 November 2024; date of current version 6 March 2025. The fundamental research described in this paper was supported, in part, by the Ministero dell'Università e della Ricerca and NextGenerationEU under Grant No. 2022JES5S2, by the National Science Foundation under Grant No. CCF-1956211, and by the Robert R. Taylor Professorship. The material in this paper was presented, in part, at the IEEE Global Communications Conference, Rio de Janeiro, Brazil, December 2022 [DOI: 10.1109/GLOBECOM48099.2022.10001626], and at the IEEE International Conference on Communications, Rome, Italy, May 2023 [DOI: 10.1109/ICC45041.2023.10279710]. *(Corresponding author: Andrea Conti.)*

Andrea Giani is with the Department of Engineering and CNIT, University of Ferrara, 44122 Ferrara, Italy, and also with the Wireless Information and Network Sciences Laboratory, Massachusetts Institute of Technology, Cambridge, MA 02139 USA (e-mail: andrea.giani@unife.it).

Moe Z. Win is with the Laboratory for Information and Decision Systems, Massachusetts Institute of Technology, Cambridge, MA 02139 USA (e-mail: moewin@mit.edu).

Andrea Conti is with the Department of Engineering and CNIT, University of Ferrara, 44122 Ferrara, Italy (e-mail: a.conti@ieee.org).

Digital Object Identifier 10.1109/JSAIT.2024.3491692

However, the development of QSC with non-Gaussian states is hindered by the lack of a theoretical foundation, which can be used to determine performance benchmarks and to guide the system design. The fundamental questions related to the design of QSC systems with non-Gaussian states are: (i) which classes of non-Gaussian states are more suitable for QSC; and (ii) how may such classes of states be characterized and then employed in QSC systems? The answers to these questions provide insights for the design of QSC systems with non-Gaussian states. The goal of this paper is to introduce the use of PVGSs for unleashing QSC. This paper establishes a theoretical foundation for QSC with PVGSs, accommodating for noise in state preparation, and shows how to exploit such class of states for different QSC applications. In particular, the key contributions are summarized as follows:

- we determine equivalence conditions for Gaussian states obtained from arbitrary permutations of rotation, displacement, and squeezing operators;
- we characterize PVGSs by deriving their Fock representation and their inner product using generalized Hermite-Kampé de Fériet (H-KdF) polynomials; and
- we explore the use of PVGSs for QSC, utilize their characterization to design QSC systems, and quantify their performance in several case studies.

The remaining sections are organized as in the following. Section II recalls generalized H-KdF polynomials and derives a closed-form expression for the generalized bilinear generating function of ordinary Hermite polynomials. Section III reviews the theory of Gaussian states, derives equivalence conditions for them, and defines PVGSs. Section IV determines the Fock representation of PVGSs. Section V derives the inner product of pure PVGSs. Section VI explores the use of PVGSs for QSC and quantifies their performance in several case studies. Finally, Section VII provides our conclusions.

Notation: Random variables are displayed in sans serif, upright fonts; their realizations in serif, italic fonts. Vectors are denoted by bold lowercase letters. Matrices and operators are denoted by bold uppercase letters. For example, a random operator and its realization are denoted by $\mathbf{X}$ and $\boldsymbol{X}$, respectively. Sets are denoted by upright sans serif font except for the sets of natural numbers, integer numbers, real numbers, and complex numbers, which are denoted by $\mathbb{N}$, $\mathbb{Z}$, $\mathbb{R}$, and $\mathbb{C}$, respectively. For $n \in \mathbb{Z}$, $\overline{n} = -$ for $n < 0$, and $\overline{n} = +$ for $n \geqslant 0$. For $x \in \mathbb{R}$, $\lfloor x \rfloor$ denotes the greatest integer less than or equal to x. For $z \in \mathbb{C}$, $|z|$ denotes its absolute value, $\angle z \in (-\pi, \pi]$ denotes its angle, z^* denotes its complex conjugate, and $\imath = \sqrt{-1}$. For $z \in \mathbb{C}$, the principal branch of the complex square root is chosen such that $\sqrt{z} = |z|^{1/2} \exp\{\imath(\angle z)/2\}$. For a matrix $\boldsymbol{M}$, $[\boldsymbol{M}]_{i,j}$ denotes the element in the i-th row and j-th column. The adjoint of an operator is denoted by $(\cdot)^\dagger$. The annihilation and the creation operators are denoted by $\boldsymbol{A}$ and $\boldsymbol{A}^\dagger$, respectively. The set of density operators defined on a Hilbert space $\mathcal{H}$ is denoted by $\mathfrak{D}(\mathcal{H})$. The identity operator defined on a Hilbert space $\mathcal{H}$ is denoted by $\boldsymbol{I}_{\mathcal{H}}$. For two operators $\boldsymbol{X}$ and $\boldsymbol{Y}$, the commutator is denoted by $[\![\boldsymbol{X}, \boldsymbol{Y}]\!]_- = \boldsymbol{X}\boldsymbol{Y} - \boldsymbol{Y}\boldsymbol{X}$. The rotation operator with parameter $\phi \in \mathbb{R}$ is $\boldsymbol{R}_\phi = \exp\{\imath\phi\boldsymbol{A}^\dagger\boldsymbol{A}\}$. The displacement operator with parameter $\mu \in \mathbb{C}$ is $\boldsymbol{D}_\mu = \exp\{\mu\boldsymbol{A}^\dagger - \mu^*\boldsymbol{A}\}$. The squeezing operator with parameter $\zeta \in \mathbb{C}$ is $\boldsymbol{S}_\zeta = \exp\{\frac{1}{2}\zeta(\boldsymbol{A}^\dagger)^2 - \frac{1}{2}\zeta^*\boldsymbol{A}^2\}$. The Pauli matrices $\boldsymbol{X}$ and $\boldsymbol{Z}$ are $\boldsymbol{X} = \left[\begin{smallmatrix} 0 & 1 \\ 1 & 0 \end{smallmatrix}\right]$ and $\boldsymbol{Z} = \left[\begin{smallmatrix} 1 & 0 \\ 0 & -1 \end{smallmatrix}\right]$, respectively.

II. Generalized Hermite-Kampé de Fériet Polynomials and Bilinear Generating Functions

This section first recalls generalized H-KdF polynomials and associated subclasses. Then, it derives a closed-form expression for the generalized bilinear generating function of ordinary Hermite polynomials [99], [100]. Such a bilinear generating function is found to play a crucial role in the characterization of PVGSs.

A. Definitions

Generalized H-KdF polynomials [101], [102], [103], [104], also referred to as generalized Hermite polynomials, are a class of polynomials that extend both two-variable H-KdF polynomials [101], [102], [103], [104] and ordinary Hermite polynomials [105], [106], [107].

Let $x, y, z, u, t \in \mathbb{C}$ and $m, n \in \mathbb{N}$. The generalized H-KdF polynomials are defined as

$$H_{m,n}(x, y; z, u\,|t) \triangleq m!n! \sum_{k=0}^{\min\{m,n\}} t^k \frac{H_{m-k}(x, y) H_{n-k}(z, u)}{k!(m-k)!(n-k)!} \tag{1}$$

where

$$H_p(\xi, w) \triangleq p! \sum_{k=0}^{\lfloor p/2 \rfloor} \frac{1}{k!(p-2k)!} \xi^{p-2k} w^k \tag{2}$$

with $p \in \mathbb{N}$, are two-variable H-KdF polynomials. Notice that ordinary Hermite polynomials are defined as

$$H_p(\xi) \triangleq p! \sum_{k=0}^{\lfloor p/2 \rfloor} \frac{(-1)^k}{k!(p-2k)!} (2\xi)^{p-2k} \tag{3}$$

and are obtained from two-variable H-KdF polynomials in (2) via the following relation

$$H_p(\xi) = H_p(2\xi, -1). \tag{4}$$

B. Generalized Bilinear Generating Function

To facilitate the characterization of PVGSs developed in the remainder of the paper, we define the function

$$G(x, y; r, s|\alpha, \beta) \triangleq \frac{1}{(1-\alpha^2)^{\frac{r+s}{2}}} M(x, y|\alpha) \times H_{r,s}\left(\frac{2(x-y\alpha)}{\sqrt{1-\alpha^2}}, -1; \frac{2(y-x\alpha)}{\sqrt{1-\alpha^2}}, -1 \,\middle|\, 2\beta\right) \tag{5}$$

where $x, y, \alpha, \beta \in \mathbb{C}, \alpha \neq 1$, $r, s \in \mathbb{N}$, and $M(x, y|\alpha)$ is the Mehler function defined as

$$M(x, y|\alpha) \triangleq \frac{1}{\sqrt{1-\alpha^2}} \exp\left(\frac{2xy\alpha - (x^2+y^2)\alpha^2}{1-\alpha^2}\right). \tag{6}$$

The following lemma uses (5) to determine a closed-form expression for the generalized bilinear generating function of ordinary Hermite polynomials.

Lemma 1: Let $x, y, t \in \mathbb{C}$, $|t| < 1$, and $r, s \in \mathbb{N}$. The generalized bilinear generating function of ordinary Hermite polynomials has the following expression

$$G(x, y; r, s|t, t) = \sum_{n=0}^{\infty} \frac{t^n}{n!\, 2^n} H_{n+r}(x) H_{n+s}(y). \tag{7}$$

Proof: See Appendix A. □

Notice that for $r = 0$ and $s = 0$, (7) reduces to

$$G(x, y; 0, 0|t, t) = M(x, y|t) = \sum_{n=0}^{\infty} \frac{t^n}{n!\, 2^n} H_n(x) H_n(y)$$

which is the standard bilinear generating function of the ordinary Hermite polynomials in (3).

III. Gaussian and Photon-Varied Gaussian States

This section reviews the theory of Gaussian states, derives equivalence conditions for Gaussian states obtained from arbitrary conventions and permutations of unitary operators, and defines the class of PVGSs.

A. Preliminaries on the Single Bosonic Mode

Consider a single bosonic mode of the quantized electromagnetic field described within an infinite dimensional Hilbert space $\mathcal{H}$ spanned by the complete orthonormal Fock basis $\{|n\rangle\}_{n\in\mathbb{N}}$, where $|n\rangle$ is the Fock state with exactly n photons. Let $\boldsymbol{Q}$ and $\boldsymbol{P}$ be the unbounded quadrature operators of the quantized field that satisfy the canonical commutation relation $[\![\boldsymbol{Q}, \boldsymbol{P}]\!]_- = \imath \boldsymbol{I}_{\mathcal{H}}$. Let $\boldsymbol{A} = (\boldsymbol{Q} + \imath \boldsymbol{P})/\sqrt{2}$ and $\boldsymbol{A}^\dagger = (\boldsymbol{Q} - \imath \boldsymbol{P})/\sqrt{2}$ be the associated bosonic annihilation and creation operators, respectively. The canonical commutation relation for $\boldsymbol{A}$ and $\boldsymbol{A}^\dagger$ is $[\![\boldsymbol{A}, \boldsymbol{A}^\dagger]\!]_- = \boldsymbol{I}_{\mathcal{H}}$. The eigenvalues and eigenvectors of the self-adjoint operator $\boldsymbol{A}^\dagger \boldsymbol{A}$, called number operator, are related by

$$\boldsymbol{A}^\dagger \boldsymbol{A}|n\rangle = n|n\rangle$$

which shows that the mean number of photons of $|n\rangle$ is $\langle n|\boldsymbol{A}^\dagger \boldsymbol{A}|n\rangle = n$.

B. Gaussian States

Gaussian states are quantum states generated by applying permutations of the unitary operators $\boldsymbol{R}_\phi$, $\boldsymbol{D}_\mu$, and $\boldsymbol{S}_\zeta$ on either the vacuum or the thermal state. Such operators can be defined according to different conventions. This paper considers the convention $\boldsymbol{R}_\phi = e^{\imath\phi \boldsymbol{A}^\dagger \boldsymbol{A}}$, $\boldsymbol{D}_\mu = e^{\mu \boldsymbol{A}^\dagger - \mu^* \boldsymbol{A}}$, and $\boldsymbol{S}_\zeta = e^{\frac{1}{2}\zeta (\boldsymbol{A}^\dagger)^2 - \frac{1}{2}\zeta^* \boldsymbol{A}^2}$. This choice is not restrictive as Gaussian states defined according to arbitrary conventions and permutations of rotation, displacement, and squeezing operators can always be written according to any other convention and permutation by properly modifying the operator parameters. We define the most general Gaussian state as

$$\boldsymbol{\Xi}(\phi, \mu, \zeta, \bar{n}) \triangleq \boldsymbol{R}_\phi \boldsymbol{D}_\mu \boldsymbol{S}_\zeta \boldsymbol{\Xi}_{\text{th}} \boldsymbol{S}_\zeta^\dagger \boldsymbol{D}_\mu^\dagger \boldsymbol{R}_\phi^\dagger \in \mathfrak{D}(\mathcal{H}) \tag{8}$$

where

$$\boldsymbol{\Xi}_{\text{th}} \triangleq \sum_{n=0}^{\infty} \frac{\bar{n}^n}{(\bar{n}+1)^{n+1}} |n\rangle\langle n| \in \mathfrak{D}(\mathcal{H}) \tag{9}$$

is the thermal state with intensity (mean number of photons) $\bar{n}$ given by the Planck law $\bar{n} = (\exp(\hbar\omega/(k_{\text{B}}T)) - 1)^{-1}$, in which $\omega, T, \hbar$, and k_{B} are respectively the angular frequency of the field, the absolute temperature, the reduced Planck constant, and the Boltzmann constant. Notice that $\boldsymbol{\Xi}(\phi, \mu, \zeta, \bar{n})$ in (8) is mixed due to $\boldsymbol{\Xi}_{\text{th}}$ being mixed when $\bar{n} > 0$. In some contexts, $\boldsymbol{\Xi}(\phi, \mu, \zeta, \bar{n})$ is also referred to as noisy Gaussian state as $\boldsymbol{\Xi}_{\text{th}}$ in (9) can model thermal fluctuations impairing the preparation of a pure Gaussian state. For $\bar{n} = 0$ (i.e., for $T \to 0$), $\boldsymbol{\Xi}_{\text{th}}$ reduces to the vacuum state and (8) results in the density operator of a pure Gaussian state, namely

$$\boldsymbol{\Xi}(\phi, \mu, \zeta, 0) = \boldsymbol{R}_\phi \boldsymbol{D}_\mu \boldsymbol{S}_\zeta |0\rangle\langle 0| \boldsymbol{S}_\zeta^\dagger \boldsymbol{D}_\mu^\dagger \boldsymbol{R}_\phi^\dagger. \tag{10}$$

The ket representation of the pure Gaussian state in (10) is

$$|\phi, \mu, \zeta\rangle \triangleq \boldsymbol{R}_\phi \boldsymbol{D}_\mu \boldsymbol{S}_\zeta |0\rangle \in \mathcal{H}. \tag{11}$$

In particular, (11) defines a pure Gaussian state according to Caves' definition [108]. An equivalent definition can be given according to Yuen as [109]

$$|\phi, \mu, \zeta\rangle = \boldsymbol{R}_\phi \boldsymbol{S}_\zeta \boldsymbol{D}_{\mu\lambda_\zeta + \mu^* \nu_\zeta} |0\rangle \tag{12}$$

where the parameters

$$\lambda_\zeta = \cosh(|\zeta|) \tag{13a}$$
$$\nu_\zeta = \sinh(|\zeta|)\, e^{\imath(\angle\zeta + \pi)} \tag{13b}$$

generate the linear transformation that maps bosonic operators $\boldsymbol{A}, \boldsymbol{A}^\dagger$ to new operators $\hat{\boldsymbol{A}}, \hat{\boldsymbol{A}}^\dagger$ according to [110, eq. (1.8)]

$$\hat{\boldsymbol{A}} = \lambda_\zeta \boldsymbol{A} - \nu_\zeta \boldsymbol{A}^\dagger \tag{14a}$$
$$\hat{\boldsymbol{A}}^\dagger = \lambda_\zeta \boldsymbol{A}^\dagger - \nu_\zeta^* \boldsymbol{A}. \tag{14b}$$

Since λ_ζ and ν_ζ satisfy $|\lambda_\zeta|^2 - |\nu_\zeta|^2 = 1$, (14) defines a canonical Bogoljubov-Valatin transformation that preserves the commutation relation, i.e., $[\![\hat{\boldsymbol{A}}, \hat{\boldsymbol{A}}^\dagger]\!]_- = [\![\boldsymbol{A}, \boldsymbol{A}^\dagger]\!]_- = \boldsymbol{I}_{\mathcal{H}}$.

An important property of Gaussian states is their closure under rotational transformations. Indeed, from the Baker-Campbell-Hausdorff formula [53], it can be found that

$$\boldsymbol{R}_\phi \boldsymbol{D}_\mu \boldsymbol{S}_\zeta = \boldsymbol{D}_{\hat{\mu}} \boldsymbol{S}_{\hat{\zeta}} \boldsymbol{R}_\phi \tag{15}$$

where

$$\hat{\mu} = \mu e^{\imath\phi} \tag{16a}$$
$$\hat{\zeta} = \zeta e^{\imath 2\phi}. \tag{16b}$$

Therefore, the mixed Gaussian state defined in (8) can equivalently be written as

$$\boldsymbol{\Xi}(\phi, \mu, \zeta, \bar{n}) = \boldsymbol{D}_{\hat{\mu}} \boldsymbol{S}_{\hat{\zeta}} \boldsymbol{\Xi}_{\text{th}} \boldsymbol{S}_{\hat{\zeta}}^\dagger \boldsymbol{D}_{\hat{\mu}}^\dagger \tag{17a}$$
$$= \boldsymbol{\Xi}(0, \hat{\mu}, \hat{\zeta}, \bar{n}) \tag{17b}$$

which is obtained by using (15), (16), and by noticing that the thermal state is invariant to rotations, i.e., $\boldsymbol{R}_\phi \boldsymbol{\Xi}_{\text{th}} \boldsymbol{R}_\phi^\dagger = \boldsymbol{\Xi}_{\text{th}}$. Analogously, a pure Gaussian state defined in (11) can equivalently be written as

$$|\phi, \mu, \zeta\rangle = \boldsymbol{D}_{\hat{\mu}} \boldsymbol{S}_{\hat{\zeta}} |0\rangle \tag{18a}$$
$$= |0, \hat{\mu}, \hat{\zeta}\rangle \tag{18b}$$

TABLE I
EQUIVALENCE CONDITIONS FOR GAUSSIAN STATES DEFINED ACCORDING TO DIFFERENT CONVENTIONS AND THOSE USED IN THIS PAPER, WHICH ARE DEFINED BY (8) AND (11) FOR MIXED AND PURE GAUSSIAN STATES, RESPECTIVELY. COEFFICIENTS λ_β AND ν_β ARE GIVEN BY (13).

Operator Chain	Transformations of ϕ,μ,ζ			Operator Chain	Transformations of ϕ,μ,ζ		
	ϕ	μ	ζ		ϕ	μ	ζ
$\boldsymbol{R}_\theta^- \boldsymbol{D}_\alpha^- \boldsymbol{S}_\beta^-$	$-\theta$	$-\alpha$	$-\beta$	$\boldsymbol{D}_\alpha^- \boldsymbol{S}_\beta^- \boldsymbol{R}_\theta^-$	$-\theta$	$-\alpha\, e^{+\imath\theta}$	$-\beta\, e^{+\imath 2\theta}$
$\boldsymbol{R}_\theta^- \boldsymbol{D}_\alpha^- \boldsymbol{S}_\beta^+$	$-\theta$	$-\alpha$	$+\beta$	$\boldsymbol{D}_\alpha^- \boldsymbol{S}_\beta^- \boldsymbol{R}_\theta^+$	$+\theta$	$-\alpha\, e^{-\imath\theta}$	$-\beta\, e^{-\imath 2\theta}$
$\boldsymbol{R}_\theta^- \boldsymbol{D}_\alpha^+ \boldsymbol{S}_\beta^-$	$-\theta$	$+\alpha$	$-\beta$	$\boldsymbol{D}_\alpha^- \boldsymbol{S}_\beta^+ \boldsymbol{R}_\theta^-$	$-\theta$	$-\alpha\, e^{+\imath\theta}$	$+\beta\, e^{+\imath 2\theta}$
$\boldsymbol{R}_\theta^- \boldsymbol{D}_\alpha^+ \boldsymbol{S}_\beta^+$	$-\theta$	$+\alpha$	$+\beta$	$\boldsymbol{D}_\alpha^- \boldsymbol{S}_\beta^+ \boldsymbol{R}_\theta^+$	$+\theta$	$-\alpha\, e^{-\imath\theta}$	$+\beta\, e^{-\imath 2\theta}$
$\boldsymbol{R}_\theta^+ \boldsymbol{D}_\alpha^- \boldsymbol{S}_\beta^-$	$+\theta$	$-\alpha$	$-\beta$	$\boldsymbol{D}_\alpha^+ \boldsymbol{S}_\beta^- \boldsymbol{R}_\theta^-$	$-\theta$	$+\alpha\, e^{+\imath\theta}$	$-\beta\, e^{+\imath 2\theta}$
$\boldsymbol{R}_\theta^+ \boldsymbol{D}_\alpha^- \boldsymbol{S}_\beta^+$	$+\theta$	$-\alpha$	$+\beta$	$\boldsymbol{D}_\alpha^+ \boldsymbol{S}_\beta^- \boldsymbol{R}_\theta^+$	$+\theta$	$+\alpha\, e^{-\imath\theta}$	$-\beta\, e^{-\imath 2\theta}$
$\boldsymbol{R}_\theta^+ \boldsymbol{D}_\alpha^+ \boldsymbol{S}_\beta^-$	$+\theta$	$+\alpha$	$-\beta$	$\boldsymbol{D}_\alpha^+ \boldsymbol{S}_\beta^+ \boldsymbol{R}_\theta^-$	$-\theta$	$+\alpha\, e^{+\imath\theta}$	$+\beta\, e^{+\imath 2\theta}$
$\boldsymbol{R}_\theta^+ \boldsymbol{D}_\alpha^+ \boldsymbol{S}_\beta^+$	$+\theta$	$+\alpha$	$+\beta$	$\boldsymbol{D}_\alpha^+ \boldsymbol{S}_\beta^+ \boldsymbol{R}_\theta^+$	$+\theta$	$+\alpha\, e^{-\imath\theta}$	$+\beta\, e^{-\imath 2\theta}$
$\boldsymbol{R}_\theta^- \boldsymbol{S}_\beta^- \boldsymbol{D}_\alpha^-$	$-\theta$	$-\alpha\lambda_\beta - \alpha^*\nu_\beta$	$-\beta$	$\boldsymbol{S}_\beta^- \boldsymbol{R}_\theta^- \boldsymbol{D}_\alpha^-$	$-\theta$	$-\alpha\lambda_\beta - \alpha^*\nu_\beta e^{\imath 2\theta}$	$-\beta\, e^{+\imath 2\theta}$
$\boldsymbol{R}_\theta^- \boldsymbol{S}_\beta^- \boldsymbol{D}_\alpha^+$	$-\theta$	$+\alpha\lambda_\beta + \alpha^*\nu_\beta$	$-\beta$	$\boldsymbol{S}_\beta^- \boldsymbol{R}_\theta^- \boldsymbol{D}_\alpha^+$	$-\theta$	$+\alpha\lambda_\beta + \alpha^*\nu_\beta e^{\imath 2\theta}$	$-\beta\, e^{+\imath 2\theta}$
$\boldsymbol{R}_\theta^- \boldsymbol{S}_\beta^+ \boldsymbol{D}_\alpha^-$	$-\theta$	$-\alpha\lambda_\beta + \alpha^*\nu_\beta$	$+\beta$	$\boldsymbol{S}_\beta^- \boldsymbol{R}_\theta^+ \boldsymbol{D}_\alpha^-$	$+\theta$	$-\alpha\lambda_\beta - \alpha^*\nu_\beta e^{-\imath 2\theta}$	$-\beta\, e^{-\imath 2\theta}$
$\boldsymbol{R}_\theta^- \boldsymbol{S}_\beta^+ \boldsymbol{D}_\alpha^+$	$-\theta$	$+\alpha\lambda_\beta - \alpha^*\nu_\beta$	$+\beta$	$\boldsymbol{S}_\beta^- \boldsymbol{R}_\theta^+ \boldsymbol{D}_\alpha^+$	$+\theta$	$+\alpha\lambda_\beta + \alpha^*\nu_\beta e^{-\imath 2\theta}$	$-\beta\, e^{-\imath 2\theta}$
$\boldsymbol{R}_\theta^+ \boldsymbol{S}_\beta^- \boldsymbol{D}_\alpha^-$	$+\theta$	$-\alpha\lambda_\beta - \alpha^*\nu_\beta$	$-\beta$	$\boldsymbol{S}_\beta^+ \boldsymbol{R}_\theta^- \boldsymbol{D}_\alpha^-$	$-\theta$	$-\alpha\lambda_\beta + \alpha^*\nu_\beta e^{\imath 2\theta}$	$+\beta\, e^{+\imath 2\theta}$
$\boldsymbol{R}_\theta^+ \boldsymbol{S}_\beta^- \boldsymbol{D}_\alpha^+$	$+\theta$	$+\alpha\lambda_\beta + \alpha^*\nu_\beta$	$-\beta$	$\boldsymbol{S}_\beta^+ \boldsymbol{R}_\theta^- \boldsymbol{D}_\alpha^+$	$-\theta$	$+\alpha\lambda_\beta - \alpha^*\nu_\beta e^{\imath 2\theta}$	$+\beta\, e^{+\imath 2\theta}$
$\boldsymbol{R}_\theta^+ \boldsymbol{S}_\beta^+ \boldsymbol{D}_\alpha^-$	$+\theta$	$-\alpha\lambda_\beta + \alpha^*\nu_\beta$	$+\beta$	$\boldsymbol{S}_\beta^+ \boldsymbol{R}_\theta^+ \boldsymbol{D}_\alpha^-$	$+\theta$	$-\alpha\lambda_\beta + \alpha^*\nu_\beta e^{-\imath 2\theta}$	$+\beta\, e^{-\imath 2\theta}$
$\boldsymbol{R}_\theta^+ \boldsymbol{S}_\beta^+ \boldsymbol{D}_\alpha^+$	$+\theta$	$+\alpha\lambda_\beta - \alpha^*\nu_\beta$	$+\beta$	$\boldsymbol{S}_\beta^+ \boldsymbol{R}_\theta^+ \boldsymbol{D}_\alpha^+$	$+\theta$	$+\alpha\lambda_\beta - \alpha^*\nu_\beta e^{-\imath 2\theta}$	$+\beta\, e^{-\imath 2\theta}$
$\boldsymbol{D}_\alpha^- \boldsymbol{R}_\theta^- \boldsymbol{S}_\beta^-$	$-\theta$	$-\alpha\, e^{+\imath\theta}$	$-\beta$	$\boldsymbol{S}_\beta^- \boldsymbol{D}_\alpha^- \boldsymbol{R}_\theta^-$	$-\theta$	$-\alpha\lambda_\beta e^{\imath\theta} - \alpha^*\nu_\beta e^{\imath\theta}$	$-\beta\, e^{+\imath 2\theta}$
$\boldsymbol{D}_\alpha^- \boldsymbol{R}_\theta^- \boldsymbol{S}_\beta^+$	$-\theta$	$-\alpha\, e^{+\imath\theta}$	$+\beta$	$\boldsymbol{S}_\beta^- \boldsymbol{D}_\alpha^- \boldsymbol{R}_\theta^+$	$+\theta$	$-\alpha\lambda_\beta e^{-\imath\theta} - \alpha^*\nu_\beta e^{-\imath\theta}$	$-\beta\, e^{-\imath 2\theta}$
$\boldsymbol{D}_\alpha^- \boldsymbol{R}_\theta^+ \boldsymbol{S}_\beta^-$	$+\theta$	$-\alpha\, e^{-\imath\theta}$	$-\beta$	$\boldsymbol{S}_\beta^- \boldsymbol{D}_\alpha^+ \boldsymbol{R}_\theta^-$	$-\theta$	$+\alpha\lambda_\beta e^{\imath\theta} + \alpha^*\nu_\beta e^{\imath\theta}$	$-\beta\, e^{+\imath 2\theta}$
$\boldsymbol{D}_\alpha^- \boldsymbol{R}_\theta^+ \boldsymbol{S}_\beta^+$	$+\theta$	$-\alpha\, e^{-\imath\theta}$	$+\beta$	$\boldsymbol{S}_\beta^- \boldsymbol{D}_\alpha^+ \boldsymbol{R}_\theta^+$	$+\theta$	$+\alpha\lambda_\beta e^{-\imath\theta} + \alpha^*\nu_\beta e^{-\imath\theta}$	$-\beta\, e^{-\imath 2\theta}$
$\boldsymbol{D}_\alpha^+ \boldsymbol{R}_\theta^- \boldsymbol{S}_\beta^-$	$-\theta$	$+\alpha\, e^{+\imath\theta}$	$-\beta$	$\boldsymbol{S}_\beta^+ \boldsymbol{D}_\alpha^- \boldsymbol{R}_\theta^-$	$-\theta$	$-\alpha\lambda_\beta e^{\imath\theta} + \alpha^*\nu_\beta e^{\imath\theta}$	$+\beta\, e^{+\imath 2\theta}$
$\boldsymbol{D}_\alpha^+ \boldsymbol{R}_\theta^- \boldsymbol{S}_\beta^+$	$-\theta$	$+\alpha\, e^{+\imath\theta}$	$+\beta$	$\boldsymbol{S}_\beta^+ \boldsymbol{D}_\alpha^- \boldsymbol{R}_\theta^+$	$+\theta$	$-\alpha\lambda_\beta e^{-\imath\theta} + \alpha^*\nu_\beta e^{-\imath\theta}$	$+\beta\, e^{-\imath 2\theta}$
$\boldsymbol{D}_\alpha^+ \boldsymbol{R}_\theta^+ \boldsymbol{S}_\beta^-$	$+\theta$	$+\alpha\, e^{-\imath\theta}$	$-\beta$	$\boldsymbol{S}_\beta^+ \boldsymbol{D}_\alpha^+ \boldsymbol{R}_\theta^-$	$-\theta$	$+\alpha\lambda_\beta e^{\imath\theta} - \alpha^*\nu_\beta e^{\imath\theta}$	$+\beta\, e^{+\imath 2\theta}$
$\boldsymbol{D}_\alpha^+ \boldsymbol{R}_\theta^+ \boldsymbol{S}_\beta^+$	$+\theta$	$+\alpha\, e^{-\imath\theta}$	$+\beta$	$\boldsymbol{S}_\beta^+ \boldsymbol{D}_\alpha^+ \boldsymbol{R}_\theta^+$	$+\theta$	$+\alpha\lambda_\beta e^{-\imath\theta} - \alpha^*\nu_\beta e^{-\imath\theta}$	$+\beta\, e^{-\imath 2\theta}$

which is obtained by using (15), (16), and by noticing that $\boldsymbol{R}_\phi|0\rangle = |0\rangle$. For pure Gaussian states defined according to Yuen, see (12), the closure under rotational transformations is preserved as

$$\begin{aligned}|\phi,\mu,\zeta\rangle &= \boldsymbol{R}_\phi \boldsymbol{S}_\zeta \boldsymbol{D}_{\mu\lambda_\zeta+\mu^*\nu_\zeta}|0\rangle \\ &= \boldsymbol{S}_{\hat\zeta} \boldsymbol{D}_{\hat\mu\lambda_{\hat\zeta}+\hat\mu^*\nu_{\hat\zeta}}|0\rangle\,. \end{aligned} \tag{19}$$

C. Equivalence Conditions for Gaussian States

In general, Gaussian states can be obtained for any permutation of rotation, displacement, and squeezing operators, which in turn can be defined according to different conventions. It is therefore desirable to establish equivalence conditions for Gaussian states obtained according to arbitrary definitions. To this aim, for $n \in \mathbb{Z}$, we introduce the following notation

$$\overline{n} \triangleq \begin{cases} - & \text{for} \quad n < 0 \\ + & \text{for} \quad n \geqslant 0 \end{cases} \tag{20}$$

which can be used to define the generalized unitary operators

$$\boldsymbol{R}_\theta^{\overline{r}} \triangleq \begin{cases} e^{-\imath\theta \boldsymbol{A}^\dagger \boldsymbol{A}} & \text{for} \quad r = -1 \\ e^{\imath\theta \boldsymbol{A}^\dagger \boldsymbol{A}} & \text{for} \quad r = +1 \end{cases} \tag{21a}$$

$$\boldsymbol{D}_\alpha^{\overline{d}} \triangleq \begin{cases} e^{\alpha^* \boldsymbol{A} - \alpha \boldsymbol{A}^\dagger} & \text{for} \quad d = -1 \\ e^{\alpha \boldsymbol{A}^\dagger - \alpha^* \boldsymbol{A}} & \text{for} \quad d = +1 \end{cases} \tag{21b}$$

$$\boldsymbol{S}_\beta^{\overline{s}} \triangleq \begin{cases} e^{\frac{1}{2}\beta^* \boldsymbol{A}^2 - \frac{1}{2}\beta (\boldsymbol{A}^\dagger)^2} & \text{for} \quad s = -1 \\ e^{\frac{1}{2}\beta (\boldsymbol{A}^\dagger)^2 - \frac{1}{2}\beta^* \boldsymbol{A}^2} & \text{for} \quad s = +1 \end{cases} \tag{21c}$$

where $r, d, s \in \{-1, +1\}$ determine the convention for rotation, displacement, and squeezing operators, respectively. Let

$$\begin{aligned}\mathcal{P} \triangleq \Big\{ &\boldsymbol{R}_\theta^{\overline{r}} \boldsymbol{D}_\alpha^{\overline{d}} \boldsymbol{S}_\beta^{\overline{s}}, \boldsymbol{R}_\theta^{\overline{r}} \boldsymbol{S}_\beta^{\overline{s}} \boldsymbol{D}_\alpha^{\overline{d}}, \boldsymbol{D}_\alpha^{\overline{d}} \boldsymbol{R}_\theta^{\overline{r}} \boldsymbol{S}_\beta^{\overline{s}}, \boldsymbol{D}_\alpha^{\overline{d}} \boldsymbol{S}_\beta^{\overline{s}} \boldsymbol{R}_\theta^{\overline{r}}, \\ &\boldsymbol{S}_\beta^{\overline{s}} \boldsymbol{R}_\theta^{\overline{r}} \boldsymbol{D}_\alpha^{\overline{d}}, \boldsymbol{S}_\beta^{\overline{s}} \boldsymbol{D}_\alpha^{\overline{d}} \boldsymbol{R}_\theta^{\overline{r}} \Big\} \end{aligned} \tag{22}$$

be the set of permutations of $\boldsymbol{R}_\theta^{\overline{r}}$, $\boldsymbol{D}_\alpha^{\overline{d}}$, and $\boldsymbol{S}_\beta^{\overline{s}}$ defined in (21). Then, generalized mixed and pure Gaussian states can be respectively defined as[1]

$$\boldsymbol{\Xi}_{\boldsymbol{G}_{\theta,\alpha,\beta}^{\overline{r},\overline{d},\overline{s}}}(\bar n) \triangleq \boldsymbol{G}_{\theta,\alpha,\beta}^{\overline{r},\overline{d},\overline{s}}\, \boldsymbol{\Xi}_{\rm th}(\boldsymbol{G}_{\theta,\alpha,\beta}^{\overline{r},\overline{d},\overline{s}})^\dagger \in \mathfrak{D}(\mathcal{H}) \tag{23a}$$

$$|\psi_{\boldsymbol{G}_{\theta,\alpha,\beta}^{\overline{r},\overline{d},\overline{s}}}\rangle \triangleq \boldsymbol{G}_{\theta,\alpha,\beta}^{\overline{r},\overline{d},\overline{s}}|0\rangle \in \mathcal{H} \tag{23b}$$

where $\boldsymbol{G}_{\theta,\alpha,\beta}^{\overline{r},\overline{d},\overline{s}} \in \mathcal{P}$. The equivalence conditions for generalized Gaussian states and those defined according to (8) and (11) are given by the Bogoljubov-Valatin transformations of ϕ, μ, and ζ that satisfy

$$\boldsymbol{R}_\phi \boldsymbol{D}_\mu \boldsymbol{S}_\zeta \boldsymbol{\Xi}_{\rm th} \boldsymbol{S}_\zeta^\dagger \boldsymbol{D}_\mu^\dagger \boldsymbol{R}_\phi^\dagger = \boldsymbol{G}_{\theta,\alpha,\beta}^{\overline{r},\overline{d},\overline{s}}\, \boldsymbol{\Xi}_{\rm th} (\boldsymbol{G}_{\theta,\alpha,\beta}^{\overline{r},\overline{d},\overline{s}})^\dagger \tag{24a}$$

[1]Notice that the Gaussian states defined in (8) and (11) are obtained by using $\boldsymbol{G}_{\phi,\mu,\zeta}^{\overline{r},\overline{d},\overline{s}} = \boldsymbol{R}_\phi^{\overline{r}} \boldsymbol{D}_\mu^{\overline{d}} \boldsymbol{S}_\zeta^{\overline{s}}$ with $r = +1$, $d = +1$, and $s = +1$.

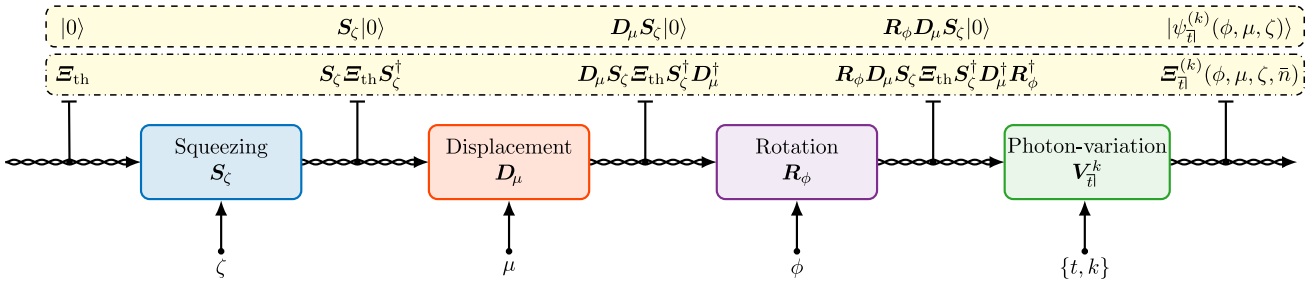

Fig. 1. Block diagram representing the sequence of operations to obtain mixed PVGSs (dashed dotted box) and pure PVGSs (dashed box), respectively defined in (27) and (29), for ζ, μ, ϕ, t, and k given as input parameters.

$$\boldsymbol{R}_\phi\boldsymbol{D}_\mu\boldsymbol{S}_\zeta|0\rangle = \boldsymbol{G}_{\theta,\alpha,\beta}^{\overline{r},\overline{d},\overline{s}}|0\rangle \tag{24b}$$

for all $r, d, s \in \{-1, +1\}$ and $\boldsymbol{G}_{\theta,\alpha,\beta}^{\overline{r},\overline{d},\overline{s}} \in \mathcal{P}$. Such transformations are listed in Table I that reports, for each convention and permutation of rotation, displacement, and squeezing operators, the transformations of ϕ, μ, and ζ that satisfy (24a) and (24b). For example, consider the mixed Gaussian state

$$\boldsymbol{\Xi}_{\boldsymbol{D}_\alpha^-\boldsymbol{S}_\beta^-\boldsymbol{R}_\theta^+}(\bar{n}) = \boldsymbol{D}_\alpha^-\boldsymbol{S}_\beta^-\boldsymbol{R}_\theta^+\boldsymbol{\Xi}_{\rm th}\big(\boldsymbol{R}_\theta^+\big)^\dagger\big(\boldsymbol{S}_\beta^-\big)^\dagger\big(\boldsymbol{D}_\alpha^-\big)^\dagger \tag{25}$$

which is obtained from (23a) with $\boldsymbol{G}_{\theta,\alpha,\beta}^{\overline{r},\overline{d},\overline{s}} = \boldsymbol{D}_\alpha^{\overline{d}}\boldsymbol{S}_\beta^{\overline{s}}\boldsymbol{R}_\theta^{\overline{r}}$ and convention determined by $r = +1$, $d = -1$, and $s = -1$. From Table I, $\boldsymbol{\Xi}_{\boldsymbol{D}_\alpha^-\boldsymbol{S}_\beta^-\boldsymbol{R}_\theta^+}(\bar{n})$ in (25) is equivalent to the Gaussian state $\boldsymbol{\Xi}(+\theta, -\alpha\, e^{-\imath 2\theta}, -\beta\, e^{-\imath 2\theta}, \bar{n})$ defined according to (8). The same approach holds for pure Gaussian states by using (23b) and (24b).

Remark 1: The equivalence conditions in Table I extend the results of this paper to any kind of Gaussian states and PVGSs. This is also important from the experimental perspective, as optical setups generating Gaussian states may be easier to implement for specific orders of rotation, displacement, and squeezing operations than for others. □

D. Photon-Varied Gaussian States

PVGSs are a subclass of PVQSs, which have been introduced in [84] to unify PAQSs and PSQSs. PVGSs can be implemented by exciting (photon-addition) or annihilating (photon-subtraction) photons from initial Gaussian states of the quantized electromagnetic field. For PVGSs, photon-addition and photon-subtraction operations are jointly described by the photon-variation operator, which is defined as

$$\boldsymbol{V}_{\bar{t}|} \triangleq \begin{cases} \boldsymbol{A} & \text{for} \quad t = -1 \quad \text{(photon-subtraction)} \\ \boldsymbol{A}^\dagger & \text{for} \quad t = +1 \quad \text{(photon-addition).} \end{cases} \tag{26}$$

For a mixed Gaussian state $\boldsymbol{\Xi}(\phi, \mu, \zeta, \bar{n}) \in \mathfrak{D}(\mathcal{H})$ defined in (8), the corresponding mixed PVGS is (see Fig. 1)

$$\boldsymbol{\Xi}_{\bar{t}|}^{(k)}(\phi, \mu, \zeta, \bar{n}) \triangleq \frac{\boldsymbol{V}_{\bar{t}|}^k\boldsymbol{\Xi}(\phi, \mu, \zeta, \bar{n})(\boldsymbol{V}_{\bar{t}|}^\dagger)^k}{N_{\bar{t}|}^{(k)}(\bar{n})} \in \mathfrak{D}(\mathcal{H}) \tag{27}$$

where k is the number of photon-variation operations (i.e., k photon-additions or k photon-subtractions) and $N_{\bar{t}|}^{(k)}(\bar{n})$ is the associated normalization constant (photon-variation is a non-unitary operation), which is given by

$$N_{\bar{t}|}^{(k)}(\bar{n}) = \mathrm{tr}\{\boldsymbol{V}_{\bar{t}|}^k\boldsymbol{\Xi}(\phi, \mu, \zeta, \bar{n})(\boldsymbol{V}_{\bar{t}|}^\dagger)^k\}. \tag{28}$$

Analogously, for a pure Gaussian state $|\phi, \mu, \zeta\rangle \in \mathcal{H}$ defined in (11), the corresponding pure PVGS is (see Fig. 1)

$$|\psi_{\bar{t}|}^{(k)}(\phi, \mu, \zeta)\rangle \triangleq \frac{1}{N_{\bar{t}|}^{(k)}}\boldsymbol{V}_{\bar{t}|}^k|\phi, \mu, \zeta\rangle \in \mathcal{H} \tag{29}$$

with associated normalization constant given by

$$N_{\bar{t}|}^{(k)} = \sqrt{\langle\zeta, \mu, \phi|(\boldsymbol{V}_{\bar{t}|}^\dagger)^k\boldsymbol{V}_{\bar{t}|}^k|\phi, \mu, \zeta\rangle}\,. \tag{30}$$

Remark 2: PVGSs extend multiple classes of quantum states. In particular, PVGSs reduce to: (i) Gaussian states when $k = 0$; (ii) photon-subtracted Gaussian states (PSGSs) [89] when $t = -1$ and $k > 0$; and (iii) photon-added Gaussian states (PAGSs) when $t = +1$ and $k > 0$. Furthermore, when $\bar{n} \to 0$, $\zeta \to 0$, and $k > 0$, PSGSs reduce to coherent states (i.e., eigenvectors of $\boldsymbol{A}$), while PAGSs reduce to photon-added coherent states [64], [86]. □

IV. Fock Representation of PVGSs

The Fock representation is fundamental for assessing the properties of quantum states. This section derives the Fock representation of PVGSs.[2]

A. Mixed PVGSs

The Fock representation of a mixed PVGS is determined in the following theorem.

Theorem 1: Let $\boldsymbol{\Xi}_{\bar{t}|}^{(k)}(\phi, \mu, \zeta, \bar{n}) \in \mathfrak{D}(\mathcal{H})$ be a mixed PVGS obtained by performing k photon-variation operations specified by t on the initial mixed Gaussian state $\boldsymbol{\Xi}(\phi, \mu, \zeta, \bar{n}) \in \mathfrak{D}(\mathcal{H})$. The Fock representation of $\boldsymbol{\Xi}_{\bar{t}|}^{(k)}(\phi, \mu, \zeta, \bar{n})$ is

$$\boldsymbol{\Xi}_{\bar{t}|}^{(k)}(\phi, \mu, \zeta, \bar{n}) = \sum_{n,m=0}^{\infty}\langle n|\boldsymbol{\Xi}_{\bar{t}|}^{(k)}(\phi, \mu, \zeta, \bar{n})|m\rangle|n\rangle\langle m|$$

where the Fock coefficients $\langle n|\boldsymbol{\Xi}_{\bar{t}|}^{(k)}(\phi, \mu, \zeta, \bar{n})|m\rangle$ and the normalization constant $N_{\bar{t}|}^{(k)}(\bar{n})$ are respectively given by (31) and (32), at the bottom of the next page, with

$$A = 1 + \bar{n} + (2\bar{n} + 1)\sinh(|\zeta|)^2 \tag{33a}$$

$$B = (2\bar{n} + 1)\sinh(|\zeta|)\cosh(|\zeta|)e^{\imath(\angle\zeta + 2\phi + \pi)} \tag{33b}$$

$$C = \frac{\bar{n}(\bar{n} + 1)}{\bar{n}^2 + (\bar{n} + \frac{1}{2})(1 + \cosh(2|\zeta|))} \tag{33c}$$

[2]For simplicity of notation, hereafter we drop the dependence on the parameters characterizing the quantum states when it is clear from the context.

$$D = \frac{\left(\bar{n}+\frac{1}{2}\right)\sinh(2|\zeta|)e^{\imath(\angle\zeta+2\phi+\pi)}}{\bar{n}^2+\left(\bar{n}+\frac{1}{2}\right)(1+\cosh(2|\zeta|))} \tag{33d}$$

$$E = e^{\imath\phi}\left[\frac{\frac{\mu}{2}+\left(\bar{n}+\frac{1}{2}\right)\mu\cosh(2|\zeta|)}{\bar{n}^2+\left(\bar{n}+\frac{1}{2}\right)(1+\cosh(2|\zeta|))} - \frac{\left(\bar{n}+\frac{1}{2}\right)\mu^*\sinh(2|\zeta|)e^{\imath\angle\zeta}}{\bar{n}^2+\left(\bar{n}+\frac{1}{2}\right)(1+\cosh(2|\zeta|))}\right] \tag{33e}$$

and $\min\{n,m\} - tk \geqslant 0$. In (32), the vector $\boldsymbol{\mu}_\phi$ is given by

$$\boldsymbol{\mu}_\phi = \begin{bmatrix}\mu e^{\imath\phi} & \mu^* e^{-\imath\phi}\end{bmatrix}^{\mathrm{T}} \tag{34}$$

whereas the matrix

$$\boldsymbol{C}_s = \begin{bmatrix}[\boldsymbol{C}_s]_{1,1} & [\boldsymbol{C}_s]_{1,2}\\ [\boldsymbol{C}_s]_{2,1} & [\boldsymbol{C}_s]_{2,2}\end{bmatrix}$$

has the following elements

$$[\boldsymbol{C}_s]_{1,1} = \frac{1}{2}[(2\bar{n}+1)\cosh(2|\zeta|) - s] \tag{35a}$$

$$[\boldsymbol{C}_s]_{1,2} = \frac{1}{2}(2\bar{n}+1)\sinh(2|\zeta|)e^{\imath(2\phi+\angle\zeta)} \tag{35b}$$

$$[\boldsymbol{C}_s]_{2,1} = \frac{1}{2}(2\bar{n}+1)\sinh(2|\zeta|)e^{-\imath(2\phi+\angle\zeta)} \tag{35c}$$

$$[\boldsymbol{C}_s]_{2,2} = \frac{1}{2}[(2\bar{n}+1)\cosh(2|\zeta|) - s] \tag{35d}$$

with $s \in \{-1,+1\}$. □

Proof: See Appendix B. ⊠

The normalization constant in (32) can also be used to determine the mean number of photons of mixed PVGSs through

$$\mathrm{tr}\{\boldsymbol{A}^\dagger\boldsymbol{A}\,\boldsymbol{\Xi}_{\overline{t}|}^{(k)}(\phi,\mu,\zeta,\bar{n})\} = \frac{N_{\overline{t}|}^{(k+1)}(\bar{n})}{N_{\overline{t}|}^{(k)}(\bar{n})} - \frac{t+1}{2}.$$

Remark 3: For $k = 0$, $\boldsymbol{\Xi}_{\overline{t}|}^{(0)}(\phi,\mu,\zeta,\bar{n}) = \boldsymbol{\Xi}(\phi,\mu,\zeta,\bar{n})$ and, from (32), $N_{\overline{t}|}^{(0)}(\bar{n}) = 1$ as required by the Gaussianity of $\boldsymbol{\Xi}(\phi,\mu,\zeta,\bar{n})$. □

As we will see in Section VI, the Fock representation is fundamental to designing QSC systems employing PVGSs. In [111] and [112], an alternative characterization of quantum states was established based on the number and distribution of the roots of their stellar representation, which is connected to their Husimi Q-function. Notice that the Husimi Q-function of the mixed PVGS $\boldsymbol{\Xi}_{\overline{t}|}^{(k)}(\phi,\mu,\zeta,\bar{n})$ is obtained from (31) as

$$Q_{\overline{t}|}^{(k)}(\xi;\phi,\mu,\zeta,\bar{n}) = \frac{1}{\pi}\sum_{n,m=0}^{\infty}\langle n|\boldsymbol{\Xi}_{\overline{t}|}^{(k)}(\phi,\mu,\zeta,\bar{n})|m\rangle\langle\xi|n\rangle\langle m|\xi\rangle$$

where $|\xi\rangle$ is a coherent state. Therefore, (31) can also be used to characterize mixed PVGSs according to [111], [112].

B. Pure PVGSs

The Fock representation of a pure PVGS is determined in the following theorem.

Theorem 2: Let $|\psi_{\overline{t}|}^{(k)}(\phi,\mu,\zeta)\rangle \in \mathcal{H}$ be the pure PVGS obtained by performing k photon-variation operations specified by t on the initial pure Gaussian state $|\phi,\mu,\zeta\rangle \in \mathcal{H}$. The Fock representation of $|\psi_{\overline{t}|}^{(k)}(\phi,\mu,\zeta)\rangle$ is given by (36), at the bottom of the page, with

$$\Lambda_{\mu,\zeta} = \sqrt{\mathrm{sech}(|\zeta|)} \times \exp\left(-\frac{1}{2}\left(|\mu|^2+(\mu^*)^2\tanh(|\zeta|)\,e^{\imath(\angle\zeta+\pi)}\right)\right) \tag{37}$$

$$\eta_{\mu,\zeta} = \frac{\mu+\mu^*\tanh(|\zeta|)\,e^{\imath(\angle\zeta+\pi)}}{\sqrt{2\tanh(|\zeta|)\,e^{\imath(\angle\zeta+\pi)}}}. \tag{38}$$

□

Proof: See Appendix C. ⊠

To complete the representation in (36), it is necessary to determine the normalization constant $N_{\overline{t}|}^{(k)}$ given by (30), which is related to the inner product $\langle\psi_{\overline{t}|}^{(k)}(\phi,\mu,\zeta)|\psi_{\overline{t}|}^{(k)}(\phi,\mu,\zeta)\rangle$. The derivation of $N_{\overline{t}|}^{(k)}$ is given in the next section where we derive the inner product of pure PVGSs.

V. Inner Product of Pure PVGSs

Pure PVGSs can also be characterized based on their orthogonality, which is of particular interest as it impacts the performance of QSC. Therefore, as will be seen in Section VI, the inner product is fundamental to designing and analyzing QSC systems. This section derives the inner product of pure PVGSs.

$$\langle n|\boldsymbol{\Xi}_{\overline{t}|}^{(k)}(\phi,\mu,\zeta,\bar{n})|m\rangle = \frac{1}{N_{\overline{t}|}^{(k)}(\bar{n})\sqrt{A^2-|B|^2}}\exp\left(-\frac{A|\mu|^2+\frac{1}{2}\left[B\left(\mu^*e^{-\imath\phi}\right)^2+B^*\left(\mu e^{\imath\phi}\right)^2\right]}{A^2-|B|^2}\right) \times\sqrt{\frac{(m!\,n!)^t}{((m-k)!\,(n-k)!)^{t+1}}}\left(\frac{D}{2}\right)^{\frac{n-tk}{2}}\left(\left(\frac{D}{2}\right)^{\frac{m-tk}{2}}\right)^* H_{m-tk,n-tk}\left(\frac{\sqrt{2}E^*}{(\sqrt{D})^*},-1;\frac{\sqrt{2}E}{\sqrt{D}},-1\middle|\frac{2C}{|D|}\right) \tag{31}$$

$$N_{\overline{t}|}^{(k)}(\bar{n}) = (-1)^k H_{k,k}\left(\left[\boldsymbol{X}\boldsymbol{Z}\boldsymbol{\mu}_\phi\right]_1,-\frac{1}{2}\left[\boldsymbol{X}\boldsymbol{Z}\boldsymbol{C}_{-t}\boldsymbol{Z}^\dagger\right]_{1,1};\left[\boldsymbol{X}\boldsymbol{Z}\boldsymbol{\mu}_\phi\right]_2,-\frac{1}{2}\left[\boldsymbol{X}\boldsymbol{Z}\boldsymbol{C}_{-t}\boldsymbol{Z}^\dagger\right]_{2,2}\middle|-\left[\boldsymbol{X}\boldsymbol{Z}\boldsymbol{C}_{-t}\boldsymbol{Z}^\dagger\right]_{1,2}\right) \tag{32}$$

$$|\psi_{\overline{t}|}^{(k)}(\phi,\mu,\zeta)\rangle = \frac{\Lambda_{\mu,\zeta}}{N_{\overline{t}|}^{(k)}}\sum_{n=0}^{\infty}\sqrt{\frac{(n+k)!}{n!\,(n-k\frac{t-1}{2})!}}\left(\frac{\tanh(|\zeta|)\,e^{\imath(\angle\zeta+2\phi+\pi)}}{2}\right)^{\frac{1}{2}\left(n-k\frac{t-1}{2}\right)} H_{n-k\frac{t-1}{2}}(\eta_{\mu,\zeta})|n+k\frac{t+1}{2}\rangle \tag{36}$$

A. Generalized Bilinear Generating Function for the Inner Product of Pure PVGSs

The following theorem establishes that the inner product of two PVGSs defines a generalized bilinear generating function of ordinary Hermite polynomials.

Theorem 3: Let $|\psi_{\overline{s}|}^{(h)}(\varphi,\xi,\omega)\rangle, |\psi_{\overline{t}|}^{(k)}(\phi,\mu,\zeta)\rangle \in \mathcal{H}$ be two PVGSs obtained from the initial Gaussian states $|\varphi,\xi,\omega\rangle$, $|\phi,\mu,\zeta\rangle \in \mathcal{H}$ by performing h and k photon-variation operations, respectively. Without loss of generality, consider $h \leqslant k$. The inner product $\langle\psi_{\overline{s}|}^{(h)}(\varphi,\xi,\omega)|\psi_{\overline{t}|}^{(k)}(\phi,\mu,\zeta)\rangle$ defines the generalized bilinear generating function of ordinary Hermite polynomials given by (39) at the bottom of the page. □

Proof: See Appendix D. ⊠

B. Expressions for the Inner Product of Pure PVGSs

The bilinear generating function associated with $\langle\psi_{\overline{s}|}^{(h)}(\varphi,\xi,\omega)|\psi_{\overline{t}|}^{(k)}(\phi,\mu,\zeta)\rangle$ in (39) can be used to obtain closed-form expressions for the inner product of: (i) two PAGSs, for $(s,t)=(+1,+1)$; (ii) a PAGS and a PSGS, for $(s,t)=(+1,-1)$; (iii) a PSGS and a PAGS, for $(s,t)=(-1,+1)$; and (iv) two PSGSs, for $(s,t)=(-1,-1)$. Let

$$\rho = \left(\sqrt{\tanh(|\omega|)\, e^{\imath(\angle\omega+2\varphi+\pi)}}\right)^{*} \sqrt{\tanh(|\zeta|)\, e^{\imath(\angle\zeta+2\phi+\pi)}}. \tag{40}$$

By specializing Theorem 3 for the aforementioned cases (i), (ii), (iii), and (iv), the following corollaries are obtained.

Corollary 1: The inner product of two PAGSs $|\psi_{+}^{(h)}(\varphi,\xi,\omega)\rangle, |\psi_{+}^{(k)}(\phi,\mu,\zeta)\rangle \in \mathcal{H}$, with $h \leqslant k$, is given by (41) at the bottom of the page. □

Proof: See Appendix E. ⊠

Corollary 2: The inner product of a PAGS $|\psi_{+}^{(h)}(\varphi,\xi,\omega)\rangle \in \mathcal{H}$ and a PSGS $|\psi_{-}^{(k)}(\phi,\mu,\zeta)\rangle \in \mathcal{H}$, with $h \leqslant k$, is given by (42) at the bottom of the page. □

Proof: See Appendix F. ⊠

Corollary 3: The inner product of a PSGS $|\psi_{-}^{(h)}(\varphi,\xi,\omega)\rangle \in \mathcal{H}$ and a PAGS $|\psi_{+}^{(k)}(\phi,\mu,\zeta)\rangle \in \mathcal{H}$, with $h \leqslant k$, is given by (43) at the bottom of the page. □

Proof: See Appendix G. ⊠

Corollary 4: The inner product of two PSGSs $|\psi_{-}^{(h)}(\varphi,\xi,\omega)\rangle, |\psi_{-}^{(k)}(\phi,\mu,\zeta)\rangle \in \mathcal{H}$, with $h \leqslant k$, is given by (44) at the bottom of the page. □

Proof: See Appendix H. ⊠

Theorem 3 facilitates the derivation of the normalization constant $N_{\overline{t}|}^{(k)}$ of a pure PVGS $|\psi_{\overline{t}|}^{(k)}(\phi,\mu,\zeta)\rangle \in \mathcal{H}$. Indeed, from the normalization condition

$$\langle\psi_{\overline{t}|}^{(k)}(\phi,\mu,\zeta)|\psi_{\overline{t}|}^{(k)}(\phi,\mu,\zeta)\rangle = 1$$

$N_{\overline{t}|}^{(k)}$ is obtained by using (41) and (44) for $t=+1$ and $t=-1$, respectively. Notice that the normalization constant of a pure PVGS is related to the normalization constant in (28) of a mixed PVGS through

$$N_{\overline{t}|}^{(k)} = \lim_{\bar{n}\to 0} \sqrt{N_{\overline{t}|}^{(k)}(\bar{n})}.$$

Remark 4: For $k=0$, the initial Gaussian state is kept untouched and, from (5), it can be easily verified that $N_{\overline{t}|}^{(0)} = 1$ as required by its Gaussianity. □

As we will see in Section VI, the inner product is fundamental to deriving the ultimate performance limits of QSC with PVGSs. Furthermore, it can also be used to determine the Husimi Q-function of pure PVGSs and to characterize them according to [111], [112]. In particular, the Husimi Q-function of a pure PVGS $|\psi_{\overline{t}|}^{(k)}(\phi,\mu,\zeta)\rangle$ is found to be

$$Q_{\overline{t}|}^{(k)}(\xi;\phi,\mu,\zeta) = \lim_{\omega\to 0} \frac{1}{\pi} |\langle\psi_{\overline{s}|}^{(0)}(0,\xi,\omega)|\psi_{\overline{t}|}^{(k)}(\phi,\mu,\zeta)\rangle|^2.$$

Therefore, when s and t are assigned, (41), (42), (43), and (44) allow one to obtain $Q_{\overline{t}|}^{(k)}(\xi;\phi,\mu,\zeta)$.

$$\langle\psi_{\overline{s}|}^{(h)}(\varphi,\xi,\omega)|\psi_{\overline{t}|}^{(k)}(\phi,\mu,\zeta)\rangle = \frac{\Lambda_{\xi,\omega}^{*}\Lambda_{\mu,\zeta}}{N_{\overline{s}|}^{(h)}N_{\overline{t}|}^{(k)}} \sum_{n=\max\{h\delta_{s,1},k\delta_{t,1}\}}^{\infty} \left[\sqrt{\frac{(n+h\delta_{s,-1})!\,(n+k\delta_{t,-1})!}{(n-h\delta_{s,1})!\,(n-sh)!\,(n-k\delta_{t,1})!\,(n-tk)!}} \times \left(\left(\frac{\tanh(|\omega|)\, e^{\imath(\angle\omega+2\varphi+\pi)}}{2}\right)^{\frac{n-sh}{2}}\right)^{*} \left(\frac{\tanh(|\zeta|)\, e^{\imath(\angle\zeta+2\phi+\pi)}}{2}\right)^{\frac{n-tk}{2}} H_{n-sh}\left(\eta_{\xi,\omega}^{*}\right) H_{n-tk}(\eta_{\mu,\zeta})\right] \tag{39}$$

$$\langle\psi_{+}^{(h)}(\varphi,\xi,\omega)|\psi_{+}^{(k)}(\phi,\mu,\zeta)\rangle = \frac{\Lambda_{\xi,\omega}^{*}\Lambda_{\mu,\zeta}}{N_{+}^{(h)}N_{+}^{(k)}} \left(\frac{\rho}{2}\right)^{h} \left(\left(\frac{\tanh(|\omega|)\, e^{\imath(\angle\omega+2\varphi+\pi)}}{2}\right)^{\frac{k-h}{2}}\right)^{*} G\left(\eta_{\xi,\omega}^{*}, \eta_{\mu,\zeta}; k, h|\rho, \rho^{-1}\right) \tag{41}$$

$$\langle\psi_{+}^{(h)}(\varphi,\xi,\omega)|\psi_{-}^{(k)}(\phi,\mu,\zeta)\rangle = \frac{\Lambda_{\xi,\omega}^{*}\Lambda_{\mu,\zeta}}{N_{+}^{(h)}N_{-}^{(k)}} \left(\frac{\tanh(|\zeta|)\, e^{\imath(\angle\zeta+2\phi+\pi)}}{2}\right)^{\frac{h+k}{2}} G\left(\eta_{\xi,\omega}^{*}, \eta_{\mu,\zeta}; 0, h+k|\rho, \rho\right) \tag{42}$$

$$\langle\psi_{-}^{(h)}(\varphi,\xi,\omega)|\psi_{+}^{(k)}(\phi,\mu,\zeta)\rangle = \frac{\Lambda_{\xi,\omega}^{*}\Lambda_{\mu,\zeta}}{N_{-}^{(h)}N_{+}^{(k)}} \left(\left(\frac{\tanh(|\omega|)\, e^{\imath(\angle\omega+2\varphi+\pi)}}{2}\right)^{\frac{h+k}{2}}\right)^{*} G\left(\eta_{\xi,\omega}^{*}, \eta_{\mu,\zeta}; h+k, 0|\rho, \rho\right) \tag{43}$$

$$\langle\psi_{-}^{(h)}(\varphi,\xi,\omega)|\psi_{-}^{(k)}(\phi,\mu,\zeta)\rangle = \frac{\Lambda_{\xi,\omega}^{*}\Lambda_{\mu,\zeta}}{N_{-}^{(h)}N_{-}^{(k)}} \left(\frac{\rho}{2}\right)^{h} \left(\frac{\tanh(|\zeta|)\, e^{\imath(\angle\zeta+2\phi+\pi)}}{2}\right)^{\frac{k-h}{2}} G\left(\eta_{\xi,\omega}^{*}, \eta_{\mu,\zeta}; h, k|\rho, \rho\right) \tag{44}$$

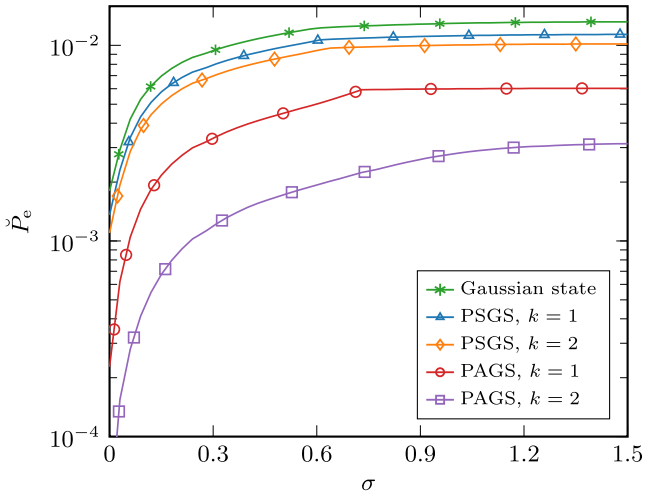

Fig. 2. Minimum DEP for the binary discrimination between a mixed PVGS, affected by phase diffusion, and the thermal state as a function of the diffusion coefficient σ. We set $\phi = 0$, $\zeta = 0.50$ and determine μ such that each state has a mean number of photons $n_{\rm p} = 10$. The thermal state has intensity $\bar{n} = 0.10$ and the prior probabilities are $p_1 = p_2 = 0.5$.

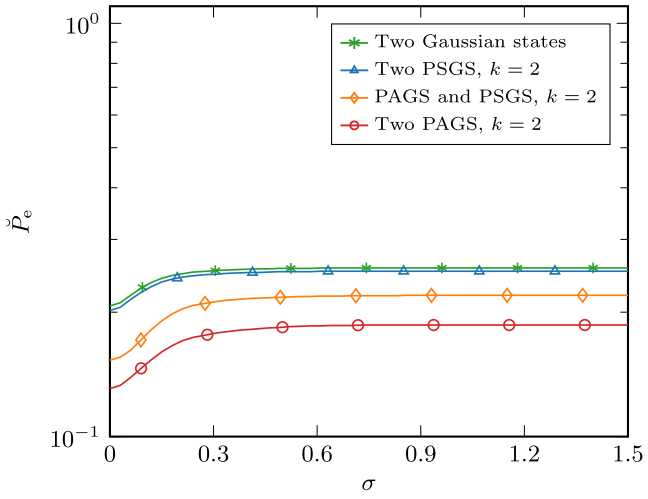

Fig. 3. Minimum DEP for the binary discrimination between two pure PVGSs, affected by phase diffusion, as a function of the diffusion coefficient σ. We set $\phi_1 = \phi_2 = 0$, $\zeta_1 = \zeta_2 = 0.25$ and determine μ_1 and μ_2 such that the two states have respectively a mean number of photons $n_{\rm p_1} = 8$ and $n_{\rm p_2} = 4$. PVGSs have $k_1 = k_2 = k = 2$ and the prior probabilities are $p_1 = p_2 = 0.5$.

VI. Quantum Sensing and Communication via PVGSs

This section explores the use of PVGSs for various QSC applications and evaluates their performance in several case studies.

A. Quantum Sensing With PVGSs

Quantum sensing, which is the process of measuring physical quantities of a target system by exploiting quantum mechanical properties [23], [24], [59], is essential for a wide plethora of applications including quantum illumination [21], [22], [23], [85], quantum tomography [23], and quantum metrology [23], [24], [25], [26], [113]. In such applications, the quantity of interest is measured based on the interaction between a quantum sensing system and the target system. Specifically, after the interaction, the final state of the quantum sensor contains information about the quantity of interest. However, due to the stochastic nature of quantum interactions, the final state cannot be deterministically identified. To address this problem, we consider quantum state discrimination (QSD) [41], [86], [114], [115], [116]. The sensing performance is related to the discrimination error probability (DEP), which depends on the quantum states used for sensing. In the literature, QSD was considered for photon-added coherent state [86] and PSGSs [89]. However, a complete characterization of QSD with PVGSs has been missing until now. In the following, we explore QSD with PVGSs. Let

$$\mathcal{S} \triangleq \left\{ \boldsymbol{\Xi}^{(k_i)}_{\overline{t_i|}}(\phi_i, \mu_i, \zeta_i, \bar{n});\ i = 1, 2, \ldots, M \right\} \subset \mathfrak{D}(\mathcal{H}) \quad (45)$$

be a set of M PVGSs, representing the initial states of a quantum sensor, respectively with prior probability $p_1, p_2, \ldots, p_M$ satisfying $\sum_{i=1}^{M} p_i = 1$. The interaction between the sensor and the target system can be modeled as the mapping

$$\mathcal{T} : \mathcal{S} \longrightarrow \grave{\mathcal{S}}$$

$$\boldsymbol{\Xi}^{(k_i)}_{\overline{t_i|}}(\phi_i, \mu_i, \zeta_i, \bar{n}) \longmapsto \boldsymbol{\Upsilon}^{(k_i)}_{\overline{t_i|}}(\phi_i, \mu_i, \zeta_i, \bar{n}) \quad (46)$$

for $i = 1, 2, \ldots, M$, where $\grave{\mathcal{S}} \subset \mathfrak{D}(\mathcal{H})$ is the set of quantum states resulting from the interaction between the initial PVGSs and the target system. Therefore, the QSD problem is formulated for quantum states in $\grave{\mathcal{S}}$. Let $\boldsymbol{\Upsilon}^{(k)}_{\overline{t|}}(\phi, \mu, \zeta, \bar{n}) \in \grave{\mathcal{S}}$ be the unknown random state of the quantum sensor after the interaction, the QSD problem can be formulated as a M-ary hypothesis testing problem where the i-th hypothesis is

$$H_i : \boldsymbol{\Upsilon}^{(k)}_{\overline{t|}}(\phi, \mu, \zeta, \bar{n}) = \boldsymbol{\Upsilon}^{(k_i)}_{\overline{t_i|}}(\phi_i, \mu_i, \zeta_i, \bar{n})$$

for $i = 1, 2, \ldots, M$. The QSD performance is quantified by the DEP, i.e., the probability of incorrectly discriminating $\boldsymbol{\Upsilon}^{(k)}_{\overline{t|}}(\phi, \mu, \zeta, \bar{n})$. A case of particular interest is the binary ($M = 2$) QSD, namely when $\boldsymbol{\Upsilon}^{(k)}_{\overline{t|}}(\phi, \mu, \zeta, \bar{n})$ has to be discriminated among the binary set $\grave{\mathcal{S}} = \{\boldsymbol{\Upsilon}^{(k_1)}_{\overline{t_1|}}(\phi_1, \mu_1, \zeta_1, \bar{n}), \boldsymbol{\Upsilon}^{(k_2)}_{\overline{t_2|}}(\phi_2, \mu_2, \zeta_2, \bar{n})\}$.[3] According to the optimal binary discrimination strategy, the minimum achievable DEP is given by [41]

$$\breve{P}_{\rm e} = \frac{1}{2}\left(1 - ||\boldsymbol{\Delta}||_1\right) \quad (47)$$

where $||\cdot||_1 = \mathrm{tr}\{\sqrt{(\cdot)^\dagger(\cdot)}\}$ denotes the trace-norm and $\boldsymbol{\Delta} = p_2 \boldsymbol{\Upsilon}^{(k_2)}_{\overline{t_2|}}(\phi_2, \mu_2, \zeta_2, \bar{n}) - p_1 \boldsymbol{\Upsilon}^{(k_1)}_{\overline{t_1|}}(\phi_1, \mu_1, \zeta_1, \bar{n})$. Note that (47) can be evaluated using the Fock representation of the states $\boldsymbol{\Upsilon}^{(k_i)}_{\overline{t_i|}}(\phi_i, \mu_i, \zeta_i, \bar{n})$, which is related to the Fock representation (31) of the initial PVGSs $\boldsymbol{\Xi}^{(k_i)}_{\overline{t_i|}}(\phi_i, \mu_i, \zeta_i, \bar{n})$. The ultimate performance limit for binary QSD is obtained from (47) by considering an ideal interaction, i.e., $\mathcal{T} = \boldsymbol{I}_{\mathcal{H}}$

[3] Examples of quantum sensing applications that rely on binary QSD are quantum illumination and signal detection. In the former, hypotheses are associated with the presence or the absence of a target. In the latter, hypotheses describe the detection of the signal state or the background state.

in (46),[4] and pure PVGSs, i.e., $\bar{n} = 0$. In this case, $\breve{P}_{\rm e}$ becomes

$$\breve{P}_{\rm e} = \frac{1 - \sqrt{1 - 4p_1p_2|\langle\psi_{\overline{t_1|}}^{(k_1)}(\phi_1,\mu_1,\zeta_1)|\psi_{\overline{t_2|}}^{(k_2)}(\phi_2,\mu_2,\zeta_2)\rangle|^2}}{2} \tag{48}$$

and depends on the inner product of the two pure PVGSs.

To evaluate the performance of PVGSs, we consider a binary QSD problem for a scenario in which the interaction between the quantum sensor and the target system is modeled as a phase diffusion process, which can be used to describe decoherence caused by a scattering process. Phase diffusion relates $\boldsymbol{\Upsilon}_{\overline{t_i|}}^{(k_i)}(\phi_i,\mu_i,\zeta_i,\bar{n})$ and $\boldsymbol{\Xi}_{\overline{t_i|}}^{(k_i)}(\phi_i,\mu_i,\zeta_i,\bar{n})$ via [117]

$$\langle n|\boldsymbol{\Upsilon}_{\overline{t_i|}}^{(k_i)}(\phi_i,\mu_i,\zeta_i,\bar{n})|m\rangle = e^{-(n-m)^2\sigma^2} \times \langle n|\boldsymbol{\Xi}_{\overline{t_i|}}^{(k_i)}(\phi_i,\mu_i,\zeta_i,\bar{n})|m\rangle \tag{49}$$

for $i = 1,2$, where $\sigma \geqslant 0$ denotes the diffusion coefficient shaping the exponential decay of off-diagonal Fock coefficients of initial PVGSs. Notice that, from (49), the Fock representation of PVGSs derived in Section IV is fundamental to determining the Fock representation of $\boldsymbol{\Upsilon}_{\overline{t_i|}}^{(k_i)}(\phi_i,\mu_i,\zeta_i,\bar{n})$.

Fig. 2 shows the minimum DEP as a function of σ when discriminating between a mixed PVGS and the thermal state in the presence of phase diffusion. Notice that PVGSs always outperform the Gaussian state. In particular, the performance improves with the number of photon-variations and degrades with the diffusion coefficient. For each PVGS setting, there exists a threshold for σ above which $\breve{P}_{\rm e}$ approaches a horizontal asymptote. This can be attributed to the fact that when σ is large, the Fock coefficients outside the diagonal are strongly attenuated by the exponential decay in (49). Fig. 2 also shows that the performance improvement of PAGSs over the Gaussian state is larger than that of PSGSs. This is due to the fact that for squeezing $\zeta = 0.50$, the benefits of photon-subtraction vanish since PSGSs approach coherent states, which are invariant to photon-subtractions. Therefore, the use of PSGSs is recommended only for large squeezing.

Similar considerations hold for Fig. 3, which shows the minimum DEP as a function of σ when discriminating between two pure ($\bar{n} = 0$) PVGSs obtained by performing two photon-variations and affected by phase diffusion. As in Fig. 2, PVGSs always outperform Gaussian states, with significant performance gain when discriminating between a PAGS and a PSGS and, especially, between two PAGSs. Notice that, despite $\bar{n} = 0$, $\breve{P}_{\rm e}$ is higher than that shown in Fig. 2. This can be attributed to the fact that the two PVGSs, with intensity $n_{\rm p1} = 8$ and $n_{\rm p2} = 4$, are less distinguishable compared to the scenario discussed in Fig. 2.

Finally, notice that the results discussed in Fig. 2 and Fig. 3 also show that PVGSs facilitate more reliable quantum communications than Gaussian states. Indeed, classical information, represented by digital symbols with known prior probabilities, can be properly encoded into PVGSs propagating through a quantum channel (modeled analogously to (46)) to the destination. Then, the quantum receiver can perform QSD to identify the transmitted PVGSs and retrieve the encoded symbols. In this case, the DEP takes the role of the symbol error probability. Therefore, $\breve{P}_{\rm e}$ shown in Fig. 2 and Fig. 3 can be respectively interpreted as the minimum symbol error probability of an on-off keying quantum communication and of a two-level quantum communication in the presence of phase diffusion (e.g., caused by scattering in optical fibers).

B. Quantum Key Distribution With PVGSs

Quantum key distribution (QKD) [118], [119], [120], [121], [122], [123], [124] is crucial for secure quantum communications and allows two parties, commonly referred to as Alice and Bob, to generate and exchange theoretically secure cryptographic keys by exploiting properties of quantum mechanics. Widely adopted metrics to assess the QKD performance are the transmission distance and secure key generation rate.

In discrete-variable QKD (DV-QKD) protocols, Alice exploits the particle nature of light to encode the information into qubits, for example realized as the polarization of photons. The security of such protocols relies on the fact that Alice employs an ideal single-photon light source. However, practical implementations of such sources exhibit a non-zero probability of generating undesired vacuum and multi-photon radiations. Vacuum radiations reduce the secure key generation rate as no information is transmitted, while multi-photon radiations can be exploited by an eavesdropper Eve to extract information about the key, thus harming the unconditional security of QKD [125], [126], [127]. Such a problem is exacerbated in scenarios with lossy quantum channels. This calls for more robust protocol variants, such as the widely adopted decoy-state protocol [128], [129], [130], [131]. The idea behind the decoy-state protocol is that Alice employs two light sources, namely signal source and decoy source, with slightly different intensities so that the emitted radiations cannot be distinguished by Eve. This strategy allows Alice and Bob to detect Eve by comparing measured and theoretical statistics of decoy radiations.

Developing QKD with the decoy-state protocol requires the design of strong sub-Poissonian signal and decoy light sources. However, in typical implementations using weak Gaussian states, the secure key generation rate is limited by the high vacuum emission probability. The use of PVGSs in DV-QKD was explored for subclasses of PAGSs [92], [93], [94]. In the following, we characterize DV-QKD with PVGSs and show that using weak PVGSs can provide better QKD performance

[4] All interactions $\mathcal{T}$ are (non-strictly) contractive in the trace-norm. Therefore, the output states of any interaction will be closer in trace-norm distance than the input ones, thus resulting in a worse $\breve{P}_{\rm e}$. The ideal interaction $\mathcal{T} = \boldsymbol{I}_{\mathcal{H}}$, however, is an isometry so it leads to achieving (48).

State	k	$P^{(k)}_{\overline{\mathrm{I}},0}$	$P^{(k)}_{\overline{\mathrm{I}},1}$	$\sum_{n\geqslant 2} P^{(k)}_{\overline{\mathrm{I}},n}$
Gaussian	0	0.39	0.28	0.33
PSGS	1	0.36	0.32	0.32
PSGS	2	0.37	0.30	0.33
PAGS	1	0	0.89	0.11

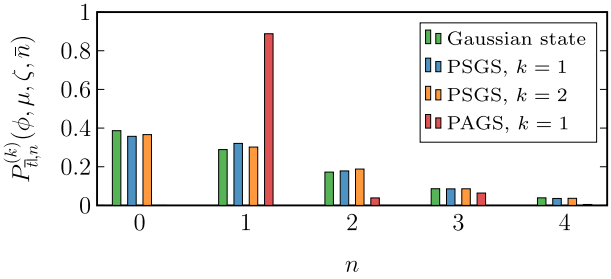

Fig. 4. Photon number distribution of a light source producing Gaussian states and PVGSs with $\bar{n}=0$, $\phi=0$, $\zeta=0.20$, and μ chosen such that the states have $n_{\mathrm{p}}=1.20$. The table reports vacuum, single-photon, and multi-photon emission probabilities; the histogram depicts the dominant terms of the photon number distribution.

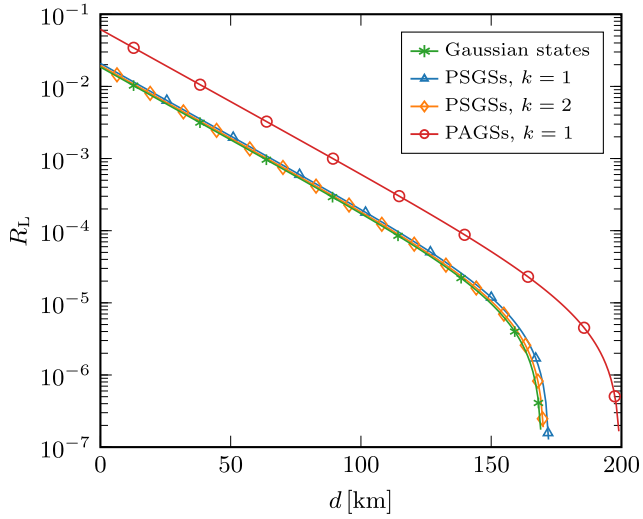

Fig. 5. Lower bound on the secure key generation rate of the decoy-state protocol as a function of the transmission distance using Gaussian states and PVGSs. Signal states' parameters are the same used for the scenario in Fig. 4. Regarding decoy states' parameters, we set $\phi=0$, $\zeta=0.20$ and determine μ to guarantee $n_{\mathrm{p}}=1.15$.

than using weak Gaussian states with the same intensity. The stochastic photon emission of a light source producing PVGSs obeys the corresponding photon number distribution given by the diagonal elements of the associated Fock representation, namely (31) and (36) for mixed and pure PVGSs, respectively. The photon number distribution of a mixed PVGS is given by

$$P^{(k)}_{\overline{\mathrm{I}},n}(\phi,\mu,\zeta,\bar{n}) = \langle n|\boldsymbol{\Xi}^{(k)}_{\overline{\mathrm{I}}}(\phi,\mu,\zeta,\bar{n})|n\rangle \tag{50}$$

which describes how likely a light source producing PVGSs emits radiations with n photons. In particular, (50) shows that the stochastic photon emission can be engineered by tuning ω, T (both determine $\bar{n}$ through the Planck law), k, ϕ, μ, and ζ. From (50), the probabilities of emitting vacuum, single-photon, and multi-photon radiations are respectively $P^{(k)}_{\overline{\mathrm{I}},0}(\phi,\mu,\zeta,\bar{n})$, $P^{(k)}_{\overline{\mathrm{I}},1}(\phi,\mu,\zeta,\bar{n})$, and $\sum_{n\geqslant 2} P^{(k)}_{\overline{\mathrm{I}},n}(\phi,\mu,\zeta,\bar{n})$.

Fig. 4 shows the photon number distribution of Gaussian states and PVGSs with $\bar{n}=0$, $\phi=0$, $\zeta=0.20$, and μ chosen such that the states have a mean number of photons $n_{\mathrm{p}}=1.20$. In particular, the table reports the probabilities of emitting vacuum, single-photon, and multi-photon radiations, while the histogram represents the dominant terms of the photon number distribution. Notice that photon-variation operations reduce the vacuum emission probability in favor of a higher single-photon probability, thus being beneficial to the secure key generation rate. Note also that PAGSs with $k=1$ are strong sub-Poissonian with $P^{(k)}_{+,1}(\phi,\mu,\zeta,\bar{n})=0.89$ due the photon-addition, which eliminates the vacuum and reduces the multi-photon emission probability. Therefore, we expect that PAGSs provide better QKD performance than PSGSs and Gaussian states. However, the use of PAGSs with $k\geqslant 2$ is forbidden in order to have a non-zero single-photon probability. Otherwise, PAGSs would emit only multi-photon radiations, thus compromising the QKD security. This restriction does not apply for PSGSs. Nonetheless, PSGSs with $k=2$ exhibit higher vacuum probability and lower single-photon probability than PSGSs with $k=1$.

To assess the performance of QKD employing PVGSs, we evaluate the lower bound on the secure key generation rate of the decoy state protocol with a single decoy as [130]

$$R_{\mathrm{L}} = \frac{1}{2}\Big(-Q_{\mathrm{g}} f_{\mathrm{e}} h_2(R_{\mathrm{e}}) + \tilde{P}^{(k)}_{\overline{\mathrm{I}},1} Y_1 [1-h_2(e_1)]\Big) \tag{51}$$

where Q_{g} is the overall gain for the signal source, f_{e} is the bidirectional error correction efficiency, $h_2(\cdot)$ is the binary entropy function, R_{e} is the total error rate, $\tilde{P}^{(k)}_{\overline{\mathrm{I}},1}$ is the single-photon emission probability for signal PVGSs, Y_1 is the detection probability conditioned to the event that Alice sent a single-photon radiation, and e_1 is the error rate associated with single-photon radiations. Consider a non-ideal optical fiber-based quantum channel operating at wavelength $\lambda = 1550\,\mathrm{nm}$ with attenuation coefficient $0.2\,\mathrm{dB/km}$, which introduces photon-loss during propagation, and an imperfect detection system with parameters given in [132].

Fig. 5 shows the lower bound on the secure key generation rate of the decoy-state protocol with Gaussian states and PVGSs as a function of the transmission distance. Notice that, as we expected in light of considerations on Fig. 4, PAGSs outperform both PSGSs and Gaussian states. This can be attributed to the fact that the photon-addition operation eliminates the vacuum emission and increases the single-photon emission probability at the expense of the multi-photon one. On the other hand, PSGSs perform slightly better than Gaussian states due to the small reduction of the vacuum emission probability in favor of the single-photon one. However, PSGSs with $k=1$ perform better than PSGSs with $k=2$ due to the higher single-photon emission probability.

VII. Conclusion

This paper established a theoretical foundation for QSC employing PVGSs, accommodating for noise in state preparation. We characterized PVGSs by deriving their Fock representation and their inner product using generalized H-KdF polynomials. We also determined equivalence conditions for Gaussian states obtained from arbitrary permutations of rotation, displacement, and squeezing operators. Finally, we explored the use of PVGSs for QSC, utilized their characterization to design QSC systems, and quantified their performance in several case studies. Numerical results show that using PVGSs for QSC can provide significant performance improvements compared to Gaussian states. The findings of this paper pave the way for the development of QSC with non-Gaussian states.

Appendix A
Proof of Lemma 1

Let $x, y, z, u, t \in \mathbb{C}$, $|t| < 1$, and $m, n \in \mathbb{N}$. By substituting (4) in (1) with $y = -1$ and $u = -1$, we have

$$H_{m,n}(2x, -1; 2z, -1\,|t) = \sum_{k=0}^{\min\{m,n\}} \binom{m}{k}\binom{n}{k} t^k k! H_{m-k}(x) H_{n-k}(z)\,. \quad (52)$$

Now, by using [133, eq. (4.1)], the right-hand side of (7) can be written as (53) at the bottom of the page. Finally, (7) follows by using (6), (52), and (5) in (53).

Appendix B
Proof of Theorem 1

Let $\boldsymbol{\Xi}(\phi, \mu, \zeta, \bar{n}) \in \mathfrak{D}(\mathcal{H})$ be the initial Gaussian state and $\boldsymbol{\Xi}_{\bar{t}|}^{(k)}(\phi, \mu, \zeta, \bar{n}) \in \mathfrak{D}(\mathcal{H})$ the corresponding PVGS obtained by performing k photon-variation operations specified by t. From (16) and (17), it follows

$$\langle n|\boldsymbol{\Xi}_{\bar{t}|}^{(k)}(\phi, \mu, \zeta, \bar{n})|m\rangle = \langle n|\boldsymbol{\Xi}_{\bar{t}|}^{(k)}(0, \hat{\mu}, \hat{\zeta}, \bar{n})|m\rangle\,. \quad (54)$$

The definition of $\boldsymbol{V}_{\bar{t}|}$ in (26) yields

$$(\boldsymbol{V}_{\bar{t}|}^{\dagger})^k|n\rangle = \sqrt{\frac{(n - k\frac{t-1}{2})!}{(n - k\frac{t+1}{2})!}}|n - tk\rangle\,. \quad (55)$$

By using (55) in (54), we obtain (56) at the bottom of the page. Then, (31) follows by using [110, eqs. (4.4), (4.23), and (5.2)], (33), and (1) in (56). In particular, (33) is derived from [110, eqs. (2.9), (2.10), (4.9), (4.10), and (4.11)] and by noting that, from (16), $|\hat{\mu}| = |\mu|$, $|\hat{\zeta}| = |\zeta|$, and $\angle\hat{\zeta} = \angle\zeta + 2\phi$.

To complete the proof, we have to demonstrate (32). This requires deriving the covariance matrix of the initial Gaussian state. From (15), we can write

$$\boldsymbol{R}_\phi \boldsymbol{D}_\mu \boldsymbol{S}_\zeta = \boldsymbol{D}_{\mu e^{\imath\phi}} \boldsymbol{R}_\phi \boldsymbol{S}_{|\zeta| e^{\imath\angle\zeta}} \quad (57a)$$

$$= \boldsymbol{D}_{\mu e^{\imath\phi}} \boldsymbol{R}_{\phi + \frac{\angle\zeta}{2}} \boldsymbol{S}_{|\zeta|} \boldsymbol{R}_{-\frac{\angle\zeta}{2}} \quad (57b)$$

where (57b) follows from (57a) by using $\boldsymbol{S}_\zeta = \boldsymbol{R}_{\frac{\angle\zeta}{2}} \boldsymbol{S}_{|\zeta|} \boldsymbol{R}_{\frac{\angle\zeta}{2}}^{\dagger}$, $\boldsymbol{R}_\phi \boldsymbol{R}_{\frac{\angle\zeta}{2}} = \boldsymbol{R}_{\phi + \frac{\angle\zeta}{2}}$, and $\boldsymbol{R}_{\frac{\angle\zeta}{2}}^{\dagger} = \boldsymbol{R}_{-\frac{\angle\zeta}{2}}$. By using (57b) and the invariance of $\boldsymbol{\Xi}_{\text{th}}$ to rotational transformations, $\boldsymbol{\Xi}(\phi, \mu, \zeta, \bar{n})$ can equivalently be written as

$$\boldsymbol{\Xi}(\phi, \mu, \zeta, \bar{n}) = \boldsymbol{D}_{\mu e^{\imath\phi}} \boldsymbol{R}_{\phi + \frac{\angle\zeta}{2}} \boldsymbol{S}_{|\zeta|} \boldsymbol{\Xi}_{\text{th}} \boldsymbol{S}_{|\zeta|}^{\dagger} \boldsymbol{R}_{\phi + \frac{\angle\zeta}{2}}^{\dagger} \boldsymbol{D}_{\mu e^{\imath\phi}}^{\dagger}\,. \quad (58)$$

Notice that the Gaussian state in (58) has the same form as that in [52], thus allowing us to use the same approach to derive its covariance matrix. Recall that, in the Heisenberg picture, $\boldsymbol{R}_\phi$ and $\boldsymbol{S}_\zeta$ generate linear canonical Bogoljubov-Valatin transformations of the bosonic operators $\boldsymbol{A}$ and $\boldsymbol{A}^{\dagger}$. Such transformations are described in the phase space through the associated symplectic matrices. In particular, the symplectic matrices associated with $\boldsymbol{R}_{\phi + \frac{\angle\zeta}{2}}$ and $\boldsymbol{S}_{|\zeta|}$ are

$$\check{\boldsymbol{R}}_{\phi + \frac{\angle\zeta}{2}} = \begin{bmatrix} \cos(\phi + \frac{\angle\zeta}{2}) & -\sin(\phi + \frac{\angle\zeta}{2}) \\ \sin(\phi + \frac{\angle\zeta}{2}) & \cos(\phi + \frac{\angle\zeta}{2}) \end{bmatrix} \quad (59)$$

$$\check{\boldsymbol{S}}_{|\zeta|} = \begin{bmatrix} e^{|\zeta|} & 0 \\ 0 & e^{-|\zeta|} \end{bmatrix}. \quad (60)$$

Hence, by using (59) and (60), the covariance matrix of $\boldsymbol{\Xi}(\phi, \mu, \zeta, \bar{n})$ in (58) is

$$\boldsymbol{V} = \left(\bar{n} + \frac{1}{2}\right) \check{\boldsymbol{R}}_{\phi + \frac{\angle\zeta}{2}} \check{\boldsymbol{S}}_{2|\zeta|} \check{\boldsymbol{R}}_{\phi + \frac{\angle\zeta}{2}}^{\dagger}\,. \quad (61)$$

Finally, (32) follows by using [84, eqs. (14), (22), and (25a)], (61), and (1), with $\boldsymbol{\mu}_\phi$ given by (34) and $\boldsymbol{C}_s$ given by (35).

Appendix C
Proof of Theorem 2

Let $|\psi_{\bar{t}|}^{(k)}(\phi, \mu, \zeta)\rangle \in \mathcal{H}$ be the pure PVGS obtained by performing k photon-variation operations specified by t on the initial pure Gaussian state $|\phi, \mu, \zeta\rangle \in \mathcal{H}$. From (16), (18), and (29), we have

$$|\psi_{\bar{t}|}^{(k)}(\phi, \mu, \zeta)\rangle = \frac{1}{N_{\bar{t}|}^{(k)}} \boldsymbol{V}_{\bar{t}|}^k \boldsymbol{D}_{\hat{\mu}} \boldsymbol{S}_{\hat{\zeta}} |0\rangle\,. \quad (62)$$

$$\sum_{n=0}^{\infty} \frac{t^n}{n!\,2^n} H_{n+r}(x) H_{n+s}(y) = \frac{1}{(1-t^2)^{\frac{r+s+1}{2}}} \exp\left(\frac{2xyt - (x^2+y^2)t^2}{1-t^2}\right) \times \sum_{k=0}^{\min\{r,s\}} \binom{r}{k}\binom{s}{k} (2t)^k k! H_{r-k}\left(\frac{x - yt}{\sqrt{1-t^2}}\right) H_{s-k}\left(\frac{y - xt}{\sqrt{1-t^2}}\right) \quad (53)$$

$$\langle n|\boldsymbol{\Xi}_{\bar{t}|}^{(k)}(\phi, \mu, \zeta, \bar{n})|m\rangle = \frac{1}{N_{\bar{t}|}^{(k)}(\bar{n})} \sqrt{\frac{(n - k\frac{t-1}{2})!}{(n - k\frac{t+1}{2})!} \frac{(m - k\frac{t-1}{2})!}{(m - k\frac{t+1}{2})!}} \langle n - tk|\boldsymbol{D}_{\hat{\mu}} \boldsymbol{S}_{\hat{\zeta}} \boldsymbol{\Xi}_{\text{th}} \boldsymbol{S}_{\hat{\zeta}}^{\dagger} \boldsymbol{D}_{\hat{\mu}}^{\dagger}|m - tk\rangle \quad (56)$$

The definition of $\boldsymbol{V}_{\bar{t}|}$ in (26) yields

$$\boldsymbol{V}_{\bar{t}|}^{k}|n\rangle = \sqrt{\frac{(n+k\frac{t+1}{2})!}{(n+k\frac{t-1}{2})!}}|n+tk\rangle\,. \tag{63}$$

By expanding $|\psi_{\bar{t}|}^{(k)}(\phi,\mu,\zeta)\rangle$ in the Fock basis and using (63), (62) can be written as

$$|\psi_{\bar{t}|}^{(k)}(\phi,\mu,\zeta)\rangle = \frac{1}{N_{\bar{t}|}^{(k)}}\sum_{n=0}^{\infty}\Bigg[\langle n|\boldsymbol{D}_{\hat{\mu}}\boldsymbol{S}_{\hat{\zeta}}|0\rangle \times\sqrt{\frac{(n+k\frac{t+1}{2})!}{(n+k\frac{t-1}{2})!}}|n+tk\rangle\Bigg]. \tag{64}$$

By substituting $p=n+k(t-1)/2$ in (64), we obtain

$$|\psi_{\bar{t}|}^{(k)}(\phi,\mu,\zeta)\rangle = \frac{1}{N_{\bar{t}|}^{(k)}}\sum_{p=0}^{\infty}\Bigg[\langle p-k\frac{t-1}{2}|\boldsymbol{D}_{\hat{\mu}}\boldsymbol{S}_{\hat{\zeta}}|0\rangle \times\sqrt{\frac{(p+k)!}{p!}}|p+k\frac{t+1}{2}\rangle\Bigg]. \tag{65}$$

Now, by using (19) and $\boldsymbol{S}_{\hat{\zeta}}=\boldsymbol{S}_{-\hat{\zeta}}^{\dagger}$, we have that

$$\langle m|\boldsymbol{D}_{\hat{\mu}}\boldsymbol{S}_{\hat{\zeta}}|0\rangle = \langle m|\boldsymbol{S}_{-\hat{\zeta}}^{\dagger}\boldsymbol{D}_{\hat{\mu}\lambda_{\hat{\zeta}}+\hat{\mu}^{*}\nu_{\hat{\zeta}}}|0\rangle\,. \tag{66}$$

In particular, (66) gives the m-th Fock coefficient of a Yuen's squeezed coherent state with displacement parameter $\hat{\mu}\lambda_{\hat{\zeta}}+\hat{\mu}^{*}\nu_{\hat{\zeta}}$ and squeezing parameter $-\hat{\zeta}$ [109]. Finally, by using (66) in (65) with $m=p-k(t-1)/2$ as well as [109, eq. (3.23)], [134, eq. (3.4)], (16), (37), and (38), we obtain (36).

Appendix D
Proof of Theorem 3

Let $|\psi_{\bar{s}|}^{(h)}(\varphi,\xi,\omega)\rangle, |\psi_{\bar{t}|}^{(k)}(\phi,\mu,\zeta)\rangle \in \mathcal{H}$ be the two PVGSs obtained from the initial Gaussian states $|\varphi,\xi,\omega\rangle, |\phi,\mu,\zeta\rangle \in \mathcal{H}$, with $h\leqslant k$. By using (36), the inner product can be written as in (67), at the bottom of the page, where we used the definition of the Kronecker delta to write $\delta_{s,1}=(s+1)/2$, $\delta_{t,1}=(t+1)/2$, $\delta_{s,-1}=-(s-1)/2$, and $\delta_{t,-1}=-(t-1)/2$.

Now, define $p=m+h\delta_{s,1}$ and $q=n+k\delta_{t,1}$, from which follow $m+h\delta_{s,-1}=p-h(\delta_{s,1}-\delta_{s,-1})=p-sh$; $m+h=p-h(\delta_{s,1}-1)=p+h\delta_{s,-1}$; $n+k\delta_{t,-1}=q-k(\delta_{t,1}-\delta_{t,-1})=q-tk$; and $n+k=q-k(\delta_{t,1}-1)=q+k\delta_{t,-1}$. By using such relations together with the orthonormality of the Fock states, (39) follows from (67) after some algebra.

Appendix E
Proof of Corollary 1

By using $(s,t)=(+1,+1)$, the substitution $q=n-\max\{h\delta_{s,1},k\delta_{t,1}\}=n-k$, (7), and (5) in (39), we obtain (68) shown at the bottom of the page. By exploiting generalized Leibniz's differentiation rule and the recursive derivative formula for ordinary Hermite polynomials, together with [135, eqs. (40) and (41)], (1), (40), and (5), we obtain (41). Notice that, as required in (7), (41) is well defined as $|\rho|<1$.

Appendix F
Proof of Corollary 2

By using $(s,t)=(+1,-1)$ and the substitution $q=n-\max\{h\delta_{s,1},k\delta_{t,1}\}=n-h$ in (39), we obtain, after some algebra, the following bilinear generating function

$$\langle\psi_{+}^{(h)}(\varphi,\xi,\omega)|\psi_{-}^{(k)}(\phi,\mu,\zeta)\rangle = \frac{\Lambda_{\xi,\omega}^{*}\Lambda_{\mu,\zeta}}{N_{+}^{(h)}N_{-}^{(k)}}\left(\frac{\tanh(|\zeta|)\,e^{\imath(\angle\zeta+2\phi+\pi)}}{2}\right)^{\frac{h+k}{2}} \times\sum_{q=0}^{\infty}\frac{\rho^{q}}{q!\,2^{q}}H_{q}\big(\eta_{\xi,\omega}^{*}\big)H_{q+h+k}(\eta_{\mu,\zeta})\,. \tag{69}$$

Then, by using (5), (40), and (7) in (69), we obtain (42). The convergence of (69) to (42) is ensured as $|\rho|<1$.

Appendix G
Proof of Corollary 3

By using $(s,t)=(-1,+1)$ and the substitution $q=n-\max\{h\delta_{s,1},k\delta_{t,1}\}=n-k$ in (39), we obtain, after some algebra, the following bilinear generating function

$$\langle\psi_{-}^{(h)}(\varphi,\xi,\omega)|\psi_{+}^{(k)}(\phi,\mu,\zeta)\rangle = \frac{\Lambda_{\xi,\omega}^{*}\Lambda_{\mu,\zeta}}{N_{-}^{(h)}N_{+}^{(k)}}\left(\left(\frac{\tanh(|\omega|)\,e^{\imath(\angle\omega+2\varphi+\pi)}}{2}\right)^{\frac{h+k}{2}}\right)^{*}$$

$$\langle\psi_{\bar{s}|}^{(h)}(\varphi,\xi,\omega)|\psi_{\bar{t}|}^{(k)}(\phi,\mu,\zeta)\rangle = \frac{\Lambda_{\xi,\omega}^{*}\Lambda_{\mu,\zeta}}{N_{\bar{s}|}^{(h)}N_{\bar{t}|}^{(k)}}\sum_{n,m=0}^{\infty}\Bigg[\sqrt{\frac{(m+h)!\,(n+k)!}{m!\,(m+h\delta_{s,-1})!\,n!\,(n+k\delta_{t,-1})!}}\left(\left(\frac{\tanh(|\omega|)\,e^{\imath(\angle\omega+2\varphi+\pi)}}{2}\right)^{\frac{m+h\delta_{s,-1}}{2}}\right)^{*} \times\left(\frac{\tanh(|\zeta|)\,e^{\imath(\angle\zeta+2\phi+\pi)}}{2}\right)^{\frac{n+k\delta_{t,-1}}{2}}H_{m+h\delta_{s,-1}}\big(\eta_{\xi,\omega}^{*}\big)H_{n+k\delta_{t,-1}}(\eta_{\mu,\zeta})\langle m+h\delta_{s,1}|n+k\delta_{t,1}\rangle\Bigg] \tag{67}$$

$$\langle\psi_{+}^{(h)}(\varphi,\xi,\omega)|\psi_{+}^{(k)}(\phi,\mu,\zeta)\rangle = \frac{\Lambda_{\xi,\omega}^{*}\Lambda_{\mu,\zeta}}{N_{+}^{(h)}N_{+}^{(k)}}\frac{1}{2^{h}(1-\rho^{2})^{\frac{k}{2}}}\left(\left(\frac{\tanh(|\omega|)\,e^{\imath(\angle\omega+2\varphi+\pi)}}{2}\right)^{\frac{k-h}{2}}\right)^{*} \times\frac{\partial^{h}}{\partial(\eta_{\xi,\omega}^{*})^{h}}\left[M\big(\eta_{\xi,\omega}^{*},\eta_{\mu,\zeta}|\rho\big)H_{k}\left(\frac{\eta_{\xi,\omega}^{*}-\eta_{\mu,\zeta}\rho}{\sqrt{1-\rho^{2}}}\right)\right] \tag{68}$$

$$\times \sum_{q=0}^{\infty} \frac{\rho^q}{q!\, 2^q} H_{q+h+k}\left(\eta^*_{\xi,\omega}\right) H_q(\eta_{\mu,\zeta}). \tag{70}$$

Then, by using (5), (40), and (7) in (70), we obtain (43). The convergence of (70) to (43) is ensured as $|\rho| < 1$.

Appendix H
Proof of Corollary 4

By using $(s,t) = (-1,-1)$ and $\max\{h\delta_{s,1}, k\delta_{t,1}\} = 0$ in (39), we obtain, after some algebra, the following bilinear generating function

$$\begin{aligned}\langle \psi^{(h)}_{-}(\varphi,\xi,\omega)|\psi^{(k)}_{-}(\phi,\mu,\zeta)\rangle &= \frac{\Lambda^*_{\xi,\omega}\Lambda_{\mu,\zeta}}{N^{(h)}_{-}N^{(k)}_{-}}\left(\frac{\rho}{2}\right)^h \left(\frac{\tanh(|\zeta|)e^{\imath(\angle\zeta+2\phi+\pi)}}{2}\right)^{\frac{k-h}{2}} \\ &\quad \times \sum_{q=0}^{\infty} \frac{\rho^q}{q!\, 2^q} H_{q+h}\left(\eta^*_{\xi,\omega}\right) H_{q+k}(\eta_{\mu,\zeta}). \end{aligned} \tag{71}$$

Then, by using (5), (40), and (7) in (71), we obtain (44). The convergence of (71) to (44) is ensured as $|\rho| < 1$.

Acknowledgment

The authors wish to thank M. Clouâtré, B. Kartal, S. Marano, and C. E. Souza for their helpful suggestions and careful reading of the paper.

References

[1] R. G. Gallager, "Low-density parity-check codes," *IRE Trans. Inf. Theory*, vol. 8, no. 1, pp. 21–28, Jan. 1962.

[2] T. Berger, Z. Zhang, and H. Viswanathan, "The CEO problem," *IEEE Trans. Inf. Theory*, vol. 42, no. 3, pp. 887–902, May 1996.

[3] S. Shamai, S. Verdú, and R. Zamir, "Systematic lossy source/channel coding," *IEEE Trans. Inf. Theory*, vol. 44, no. 2, pp. 564–579, Mar. 1998.

[4] Y. Altuğ and A. B. Wagner, "Moderate deviations in channel coding," *IEEE Trans. Inf. Theory*, vol. 60, no. 8, pp. 4417–4426, Aug. 2014.

[5] S.-Y. Li, R. Yeung, and N. Cai, "Linear network coding," *IEEE Trans. Inf. Theory*, vol. 49, no. 2, pp. 371–381, Feb. 2003.

[6] Y. Liang, H. V. Poor, and S. Shamai, "Secure communication over fading channels," *IEEE Trans. Inf. Theory*, vol. 54, no. 6, pp. 2470–2492, Jun. 2008.

[7] T. Berger, "Rate distortion theory for sources with abstract alphabets and memory," *Inf. Control*, vol. 13, no. 3, pp. 254–273, Sep. 1968.

[8] T. Berger and R. Yeung, "Multiterminal source encoding with one distortion criterion," *IEEE Trans. Inf. Theory*, vol. 35, no. 2, pp. 228–236, Mar. 1989.

[9] C. Heegard and T. Berger, "Rate distortion when side information may be absent," *IEEE Trans. Inf. Theory*, vol. 31, no. 6, pp. 727–734, Nov. 1985.

[10] Y. Steinberg and S. Verdú, "Simulation of random processes and rate-distortion theory," *IEEE Trans. Inf. Theory*, vol. 42, no. 1, pp. 63–86, Jan. 1996.

[11] A. Dembo and I. Kontoyiannis, "Source coding, large deviations, and approximate pattern matching," *IEEE Trans. Inf. Theory*, vol. 48, no. 6, pp. 1590–1615, Jun. 2002.

[12] R. Venkataramanan and S. S. Pradhan, "Source coding with feed-forward: Rate-distortion theorems and error exponents for a general source," *IEEE Trans. Inf. Theory*, vol. 53, no. 6, pp. 2154–2179, Jun. 2007.

[13] G. Balasubramanian et al., "Nanoscale imaging magnetometry with diamond spins under ambient conditions," *Nature*, vol. 455, no. 7213, pp. 648–651, Oct. 2008.

[14] T. Wild, V. Braun, and H. Viswanathan, "Joint design of communication and sensing for beyond 5G and 6G systems," *IEEE Access*, vol. 9, pp. 30845–30857, 2021.

[15] J. A. Zhang et al., "Enabling joint communication and radar sensing in mobile networks—A survey," *IEEE Commun. Surveys Tuts.*, vol. 24, no. 1, pp. 306–345, 1st Quart., 2021.

[16] C. E. Shannon, "A mathematical theory of communication," *Bell Syst. Techn. J.*, vol. 27, no. 7, pp. 379–423, 1948.

[17] R. G. Gallager, *Information Theory and Reliable Communication*, 1st ed. New York, NY, USA: Wiley, 1968.

[18] A. F. Molisch, *Wireless Communications*, 1st ed. Piscataway, NJ, USA: Wiley/IEEE Press, 2005.

[19] J. Gibson, *The Communications Handbook* (Electrical Engineering Handbook Series). Boca Raton, FL, USA: CRC Press, 2018.

[20] U. Khalid, M. S. Ulum, M. Z. Win, and H. Shin, "Integrated satellite-ground variational quantum sensing networks," *IEEE Commun. Mag.*, vol. 62, no. 10, pp. 20–27, Oct. 2024.

[21] S. Lloyd, "Enhanced sensitivity of photodetection via quantum illumination," *Science*, vol. 321, no. 5895, pp. 1463–1465, Jan. 2008.

[22] S.-H. Tan et al., "Quantum illumination with Gaussian states," *Phys. Rev. Lett.*, vol. 101, no. 25, Dec. 2008, Art. no. 253601.

[23] C. L. Degen, F. Reinhard, and P. Cappellaro, "Quantum sensing," *Rev. Mod. Phys.*, vol. 89, no. 3, Jul. 2017, Art. no. 35002.

[24] V. Giovannetti, S. Lloyd, and L. Maccone, "Quantum-enhanced measurements: Beating the standard quantum limit," *Science*, vol. 306, no. 5700, pp. 1330–1336, Nov. 2004.

[25] U. Khalid, Y. Jeong, and H. Shin, "Measurement-based quantum correlation in mixed-state quantum metrology," *Quantum Inf. Process.*, vol. 17, no. 12, p. 343, Nov. 2018.

[26] H. Kwon, K. C. Tan, T. Volkoff, and H. Jeong, "Nonclassicality as a quantifiable resource for quantum metrology," *Phys. Rev. Lett.*, vol. 122, no. 4, Feb. 2019, Art. no. 40503.

[27] M. S. Ulum, U. Khalid, J. W. Setiawan, T. Q. Duong, M. Z. Win, and H. Shin, "Variational anonymous quantum sensing," *IEEE J. Sel. Areas Commun.*, vol. 42, no. 9, pp. 2275–2291, Sep. 2024.

[28] A. Furusawa, J. L. Sørensen, S. L. Braunstein, C. A. Fuchs, H. J. Kimble, and E. S. Polzik, "Unconditional quantum teleportation," *Science*, vol. 282, no. 5389, pp. 706–709, Oct. 1998.

[29] G. Cariolaro, *Quantum Communications*. Heidelberg, Germany: Springer, 2015.

[30] A. S. Fletcher, P. W. Shor, and M. Z. Win, "Optimum quantum error recovery using semidefinite programming," *Phys. Rev. A*, vol. 75, Jan. 2007, Art. no. 12338.

[31] A. S. Fletcher, P. W. Shor, and M. Z. Win, "Channel-adapted quantum error correction for the amplitude damping channel," *IEEE Trans. Inf. Theory*, vol. 54, no. 12, pp. 5705–5718, Dec. 2008.

[32] C. H. Bennett, I. Devetak, A. W. Harrow, P. W. Shor, and A. Winter, "The quantum reverse Shannon theorem and resource tradeoffs for simulating quantum channels," *IEEE Trans. Inf. Theory*, vol. 60, no. 5, pp. 2926–2959, May 2014.

[33] H. M. Garmaroudi, S. S. Pradhan, and J. Chen, "Rate-limited quantum-to-classical optimal transport: A lossy source coding perspective," in *Proc. IEEE Int. Symp. Inf. Theory*, Taipei, Taiwan, 2023, pp. 1925–1930.

[34] M. Chiani, A. Conti, and M. Z. Win, "Piggybacking on quantum streams," *Phys. Rev. A*, vol. 102, Jul. 2020, Art. no. 12410.

[35] M. Caleffi and A. S. Cacciapuoti, "Quantum switch for the quantum Internet: Noiseless communications through noisy channels," *IEEE J. Sel. Areas Commun.*, vol. 38, no. 3, pp. 575–588, Mar. 2020.

[36] R. Slusher and B. Yurke, "Squeezed light for coherent communications," *J. Lightw. Technol.*, vol. 8, no. 3, pp. 466–477, Mar. 1990.

[37] H. Yuen and J. Shapiro, "Optical communication with two-photon coherent states–Part I: Quantum-state propagation and quantum-noise," *IEEE Trans. Inf. Theory*, vol. 24, no. 6, pp. 657–668, Nov. 1978.

[38] U. Khalid, M. S. Ulum, A. Farooq, T. Q. Duong, O. A. Dobre, and H. Shin, "Quantum semantic communications for metaverse: Principles and challenges," *IEEE Wireless Commun.*, vol. 30, no. 4, pp. 26–36, Aug. 2023.

[39] W. C. Lindsey, "Transmission of classical information over noisy quantum channels—A spectrum approach," *IEEE J. Sel. Areas Commun.*, vol. 38, no. 3, pp. 427–438, Mar. 2020.

[40] S. Marano and M. Z. Win, "Distributing quantum states with finite lifetime," *Phys. Rev. A*, vol. 107, May 2023, Art. no. 52413.

[41] C. W. Helstrom, *Quantum Detection and Estimation Theory*, 1st ed. New York, NY, USA: Academic, 1976.

[42] C. W. Helstrom, J. Liu, and J. Gordon, "Quantum-mechanical communication theory," *Proc. IEEE*, vol. 58, no. 10, pp. 1578–1598, Oct. 1970.

[43] W. Dai, T. Peng, and M. Z. Win, "Optimal remote entanglement distribution," *IEEE J. Sel. Areas Commun.*, vol. 38, no. 3, pp. 540–556, Mar. 2020.

[44] M. Shtaif, C. Antonelli, and M. Brodsky, "Nonlocal compensation of polarization mode dispersion in the transmission of polarization entangled photons," *Opt. Express*, vol. 19, no. 3, pp. 1728–1733, 2011.

[45] Z. Liu, S. Marano, and M. Z. Win, "Establishing high-fidelity entanglement in quantum repeater chains," *IEEE J. Sel. Areas Commun.*, vol. 42, no. 7, pp. 1763–1778, Jul. 2024.

[46] L. Hu, M. Al-amri, Z. Liao, and M. S. Zubairy, "Continuous-variable quantum key distribution with non-Gaussian operations," *Phys. Rev. A*, vol. 102, no. 1, Jul. 2020, Art. no. 12608.

[47] M. He, R. Malaney, and J. Green, "Multimode CV-QKD with non-Gaussian operations," *Quantum Eng.*, vol. 2, no. 2, p. e40, May 2020.

[48] S. N. Paing, J. W. Setiawan, T. Q. Duong, D. Niyato, M. Z. Win, and H. Shin, "Quantum anonymous networking: A quantum leap in privacy," *IEEE Netw.*, vol. 38, no. 5, pp. 131–145, Sep./Oct. 2024.

[49] N. Cai, A. Winter, and R. W. Yeung, "Quantum privacy and quantum wiretap channels," *Probl. Inf. Transmiss.*, vol. 40, no. 4, pp. 318–336, Oct. 2004.

[50] A. Winter, "Coding theorem and strong converse for quantum channels," *IEEE Trans. Inf. Theory*, vol. 45, no. 7, pp. 2481–2485, Nov. 1999.

[51] F. Zaman, S. N. Paing, A. Farooq, H. Shin, and M. Z. Win, "Concealed quantum telecomputation for anonymous 6G URLLC networks," *IEEE J. Sel. Areas Commun.*, vol. 41, no. 7, pp. 2278–2296, Jul. 2023.

[52] C. Weedbrook et al., "Gaussian quantum information," *Rev. Mod. Phys.*, vol. 84, no. 2, pp. 621–669, May 2012.

[53] B. L. Schumaker, "Quantum mechanical pure states with Gaussian wave functions," *Phys. Rep.*, vol. 135, no. 6, pp. 317–408, Apr. 1986.

[54] R. J. Glauber, "The quantum theory of optical coherence," *Phys. Rev.*, vol. 130, no. 6, pp. 2529–2539, Jun. 1963.

[55] X.-B. Wang, T. Hiroshima, A. Tomita, and M. Hayashi, "Quantum information with Gaussian states," *Phys. Rep.*, vol. 448, no. 1, pp. 1–111, Aug. 2007.

[56] G. Adesso, S. Ragy, and A. R. Lee, "Continuous variable quantum information: Gaussian states and beyond," *Open Syst. Inf. Dyn.*, vol. 21, Jun. 2014, Art. no. 1440001.

[57] S. Lloyd and S. L. Braunstein, "Quantum computation over continuous variables," *Phys. Rev. Lett.*, vol. 82, no. 8, pp. 1784–1787, Feb. 1999.

[58] Y.-S. Ra et al., "Non-Gaussian quantum states of a multimode light field," *Nat. Phys.*, vol. 16, no. 2, pp. 144–147, Feb. 2020.

[59] G. Adesso, F. Dell'Anno, S. De Siena, F. Illuminati, and L. A. M. Souza, "Optimal estimation of losses at the ultimate quantum limit with non-Gaussian states," *Phys. Rev. A*, vol. 79, no. 4, Apr. 2009, Art. no. 40305.

[60] A. Mari and J. Eisert, "Positive Wigner functions render classical simulation of quantum computation efficient," *Phys. Rev. Lett.*, vol. 109, no. 23, Dec. 2012, Art. no. 230503.

[61] M. Walschaers, "Non-Gaussian quantum states and where to find them," *PRX Quantum*, vol. 2, no. 3, Sep. 2021, Art. no. 30204.

[62] A. Kenfack and K. Zyczkowski, "Negativity of the Wigner function as an indicator of non-classicality," *J. Opt. B, Quant. Semiclass. Opt.*, vol. 6, no. 10, pp. 396–404, Aug. 2004.

[63] G. S. Agarwal, *Quantum Optics*. Cambridge, UK: Cambridge Univ., 2012.

[64] G. S. Agarwal and K. Tara, "Nonclassical properties of states generated by the excitations on a coherent state," *Phys. Rev. A*, vol. 43, no. 1, pp. 492–497, Jan. 1991.

[65] X.-X. Xu, L.-Y. Hu, and H.-Y. Fan, "Photon-added squeezed thermal states: Statistical properties and its decoherence in a photon-loss channel," *Opt. Commun.*, vol. 283, no. 9, pp. 1801–1809, May 2010.

[66] G. S. Agarwal and K. Tara, "Nonclassical character of states exhibiting no squeezing or sub-Poissonian statistics," *Phys. Rev. A*, vol. 46, no. 1, pp. 485–488, Jul. 1992.

[67] A. Biswas and G. S. Agarwal, "Nonclassicality and decoherence of photon-subtracted squeezed states," *Phys. Rev. A*, vol. 75, no. 3, Mar. 2007, Art. no. 32104.

[68] M. S. Kim, E. Park, P. L. Knight, and H. Jeong, "Nonclassicality of a photon-subtracted Gaussian field," *Phys. Rev. A*, vol. 71, no. 4, Apr. 2005, Art. no. 43805.

[69] M. Dakna, T. Anhut, T. Opatrný, L. Knöll, and D.-G. Welsch, "Generating Schrödinger-cat-like states by means of conditional measurements on a beam splitter," *Phys. Rev. A*, vol. 55, no. 4, pp. 3184–3194, Apr. 1997.

[70] L.-Y. Hu, X.-X. Xu, Z.-S. Wang, and X.-F. Xu, "Photon-subtracted squeezed thermal state: Nonclassicality and decoherence," *Phys. Rev. A*, vol. 82, no. 4, Oct. 2010, Art. no. 43842.

[71] J. Wenger, R. Tualle-Brouri, and P. Grangier, "Non-Gaussian statistics from individual pulses of squeezed light," *Phys. Rev. Lett.*, vol. 92, no. 15, Apr. 2004, Art. no. 153601.

[72] A. Zavatta, S. Viciani, and M. Bellini, "Quantum-to-classical transition with single-photon-added coherent states of light," *Science*, vol. 306, no. 5696, pp. 660–662, Oct. 2004.

[73] A. Zavatta, V. Parigi, and M. Bellini, "Experimental nonclassicality of single-photon-added thermal light states," *Phys. Rev. A*, vol. 75, no. 5, May 2007, Art. no. 52106.

[74] A. Zavatta, S. Viciani, and M. Bellini, "Single-photon excitation of a coherent state: Catching the elementary step of stimulated light emission," *Phys. Rev. A*, vol. 72, no. 2, Aug. 2005, Art. no. 23820.

[75] A. Ourjoumtsev, A. Dantan, R. Tualle-Brouri, and P. Grangier, "Increasing entanglement between Gaussian states by coherent photon subtraction," *Phys. Rev. Lett.*, vol. 98, no. 3, Jan. 2007, Art. no. 30502.

[76] K. Wakui, H. Takahashi, A. Furusawa, and M. Sasaki, "Photon subtracted squeezed states generated with periodically poled KTiOPO4," *Opt. Exp.*, vol. 15, no. 6, pp. 3568–3574, Mar. 2007.

[77] A. Ourjoumtsev, R. Tualle-Brouri, J. Laurat, and P. Grangier, "Generating optical Schrödinger kittens for quantum information processing," *Science*, vol. 312, no. 5770, pp. 83–86, Apr. 2006.

[78] N. Namekata, Y. Takahashi, G. Fujii, D. Fukuda, S. Kurimura, and S. Inoue, "Non-Gaussian operation based on photon subtraction using a photon-number-resolving detector at a telecommunications wavelength," *Nat. Photonics*, vol. 4, no. 9, pp. 655–660, Jul. 2010.

[79] L.-Y. Hu, F. Jia, and Z.-M. Zhang, "Entanglement and nonclassicality of photon-added two-mode squeezed thermal state," *J. Opt. Soc. Am. B*, vol. 29, no. 6, pp. 1456–1464, Jun. 2012.

[80] X.-G. Meng et al., "Continuous-variable entanglement and Wigner-function negativity via adding or subtracting photons," *Annu. Phys.*, vol. 532, no. 5, May 2020, Art. no. 1900585.

[81] S. M. Barnett, G. Ferenczi, C. R. Gilson, and F. C. Speirits, "Statistics of photon-subtracted and photon-added states," *Phys. Rev. A*, vol. 98, no. 1, Jul. 2018, Art. no. 13809.

[82] P. Marian and T. A. Marian, "A geometric measure of non-classicality," *Physica Scripta*, vol. 95, no. 5, Mar. 2020, Art. no. 54005.

[83] Z. Zhang and H. Fan, "Properties of states generated by excitations on a squeezed vacuum state," *Phys. Lett. A*, vol. 165, no. 1, pp. 14–18, May 1992.

[84] S. Guerrini, M. Z. Win, and A. Conti, "Photon-varied quantum states: Unified characterization," *Phys. Rev. A*, vol. 108, Aug. 2023, Art. no. 22425.

[85] L. Fan and M. S. Zubairy, "Quantum illumination using non-Gaussian states generated by photon subtraction and photon addition," *Phys. Rev. A*, vol. 98, Jul. 2018, Art. no. 12319.

[86] S. Guerrini, M. Z. Win, M. Chiani, and A. Conti, "Quantum discrimination of noisy photon-added coherent states," *IEEE J. Sel. Areas Inf. Theory*, vol. 1, no. 2, pp. 469–479, Aug. 2020.

[87] N. Akhtar, J. Wu, J.-X. Peng, W.-M. Liu, and G. Xianlong, "Sub-Planck structures and sensitivity of the superposed photon-added or photon-subtracted squeezed-vacuum states," *Phys. Rev. A*, vol. 107, no. 5, May 2023, Art. no. 52614.

[88] S. Wang, X. Xu, Y. Xu, and L. Zhang, "Quantum interferometry via a coherent state mixed with a photon-added squeezed vacuum state," *Opt. Commun.*, vol. 444, pp. 102–110, Aug. 2019.

[89] A. Giani, M. Z. Win, and A. Conti, "Quantum discrimination of noisy photon-subtracted squeezed states," in *Proc. IEEE Glob. Telecomm. Conf.*, 2022, pp. 5826–5831.

[90] R. Birrittella and C. C. Gerry, "Quantum optical interferometry via the mixing of coherent and photon-subtracted squeezed vacuum states of light," *J. Opt. Soc. Am. B*, vol. 31, no. 3, pp. 586–593, Mar. 2014.

[91] P. V. P. Pinheiro and R. V. Ramos, "Quantum communication with photon-added coherent states," *Quantum Inf. Process.*, vol. 12, no. 1, pp. 537–547, Mar. 2013.

[92] D. Wang et al., "Quantum key distribution with the single-photon-added coherent source," *Phys. Rev. A*, vol. 90, no. 6, Dec. 2014, Art. no. 62315.

[93] A. Giani, M. Z. Win, and A. Conti, "Source engineering for quantum key distribution with noisy photon-added squeezed states," in *Proc. IEEE Int. Conf. Commun.*, 2023, pp. 4169–4174.

[94] J. Li et al., "Phase-matching quantum key distribution with the single-photon-added coherent source," *J. Opt. Soc. Am. B*, vol. 40, no. 8, pp. 2108–2113, Aug. 2023.

[95] P. Huang, G. He, J. Fang, and G. Zeng, "Performance improvement of continuous-variable quantum key distribution via photon subtraction," *Phys. Rev. A*, vol. 87, no. 1, Jan. 2013, Art. no. 12317.

[96] S. Srikara, K. Thapliyal, and A. Pathak, "Continuous variable B92 quantum key distribution protocol using single photon added and subtracted coherent states," *Quantum Inf. Process.*, vol. 19, no. 10, p. 371, Oct. 2020.

[97] E. Villaseñor, M. He, Z. Wang, R. Malaney, and M. Z. Win, "Enhanced uplink quantum communication with satellites via downlink channels," *IEEE Trans. Quantum Eng.*, vol. 2, pp. 1–18, Jun. 2021.

[98] J. Singh and S. Bose, "Non-Gaussian operations in measurement-device-independent quantum key distribution," *Phys. Rev. A*, vol. 104, no. 5, Nov. 2021, Art. no. 52605.

[99] H. Srivastava and H. Manocha, *A Treatise on Generating Functions* (British Political Sociology Yearbook). New York, NY, USA: Ellis Horwood, 1984.

[100] H. S. Wilf, *Generatingfunctionology*, 3rd ed. New York, NY, USA: K Peters/CRC Press, 2005.

[101] G. Dattoli, S. Lorenzutta, G. Maino, and A. Torre, "Theory of multiindex multivariable bessel functions and Hermite polynomials," *Le Matematiche*, vol. 52, no. 1, pp. 177–195, 1997.

[102] G. Dattoli, "Generalized polynomials, operational identities and their applications," *J. Comput. Appl. Math.*, vol. 118, nos. 1–2, pp. 111–123, Jun. 2000.

[103] D. Babusci, G. Dattoli, S. Licciardi, and E. Sabia, *Mathematical Methods for Physicists*. Singapore: World Sci., 2019.

[104] G. Dattoli and A. Torre, *Theory and Applications of Generalized Bessel Functions*. Rome, Italy: Aracne Editrice, 1996.

[105] P. Appell and J. K. de Fériet, *Fonctions Hypergéométriques et Hypersphériques; Polynômes d'Hermite*. Paris, France: Gauthier-Villars, 1926.

[106] A. Erdélyi, W. Magnus, F. Oberhettinger, F. G. Tricomi, and H. Bateman, *Higher Transcendental Functions*. New York, NY, USA: McGraw-Hill, 1953.

[107] C. Hermite, "Sur un nouveau développement en série des fonctions," *C. R. Acad. Sci.*, vol. 58, pp. 93–100, 1864.

[108] C. M. Caves, "Quantum-mechanical noise in an interferometer," *Phys. Rev. D*, vol. 23, no. 8, pp. 1693–1708, Apr. 1981.

[109] H. P. Yuen, "Two-photon coherent states of the radiation field," *Phys. Rev. A*, vol. 13, no. 6, pp. 2226–2243, Jun. 1976.

[110] P. Marian and T. A. Marian, "Squeezed states with thermal noise. I. Photon-number statistics," *Phys. Rev. A*, vol. 47, no. 5, pp. 4474–4486, May 1993.

[111] U. Chabaud and S. Mehraban, "Holomorphic representation of quantum computations," *Quantum*, vol. 6, p. 831, Oct. 2022.

[112] U. Chabaud, D. Markham, and F. Grosshans, "Stellar representation of non-Gaussian quantum states," *Phys. Rev. Lett.*, vol. 124, no. 6, Feb. 2020, Art. no. 63605.

[113] M. Paris, "Quantum estimation for quantum technology," *Int. J. Quantum Inf.*, vol. 7, no. 1, pp. 125–137, 2009.

[114] A. S. Holevo, "Statistical decision theory for quantum systems," *J. Multivar. Anal.*, vol. 3, no. 4, pp. 337–394, 1973.

[115] S. M. Barnett and S. Croke, "Quantum state discrimination," *Adv. Opt. Photon.*, vol. 1, no. 2, pp. 238–278, 2009.

[116] H. Yuen, R. S. Kennedy, and M. Lax, "Optimum testing of multiple hypotheses in quantum detection theory," *IEEE Trans. Inf. Theory*, vol. 21, no. 2, pp. 125–134, Mar. 1975.

[117] C. W. Gardiner and P. Zoller, *Quantum Noise*, 3rd ed. Berlin, Germany: Springer, 2004.

[118] C. H. Bennett and G. Brassard, "Quantum cryptography: Public key distribution and coin tossing," in *Proc. IEEE Int. Conf. Comput., Syst., Signal Process.*, 1984, pp. 175–179.

[119] L. Goldenberg, L. Vaidman, and S. Wiesner, "Quantum gambling," *Phys. Rev. Lett.*, vol. 82, no. 16, pp. 3356–3359, Apr. 1999.

[120] V. Scarani, H. Bechmann-Pasquinucci, N. J. Cerf, M. Dušek, N. Lütkenhaus, and M. Peev, "The security of practical quantum key distribution," *Rev. Mod. Phys.*, vol. 81, no. 3, pp. 1301–1350, Sep. 2009.

[121] S. Pirandola et al., "Advances in quantum cryptography," *Adv. Opt. Photon.*, vol. 12, no. 4, pp. 1012–1236, Dec. 2020.

[122] H.-K. Lo and H. F. Chau, "Unconditional security of quantum key distribution over arbitrarily long distances," *Science*, vol. 283, no. 5410, pp. 2050–2056, Mar. 1999.

[123] P. W. Shor and J. Preskill, "Simple proof of security of the BB84 quantum key distribution protocol," *Phys. Rev. Lett.*, vol. 85, no. 2, pp. 441–444, Jul. 2000.

[124] D. Gottesman, H.-K. Lo, N. Lütkenhaus, and J. Preskill, "Security of quantum key distribution with imperfect devices," *Quantum Inf. Comput.*, vol. 4, no. 5, pp. 325–360, Sep. 2004.

[125] G. Brassard, N. Lütkenhaus, T. Mor, and B. C. Sanders, "Limitations on practical quantum cryptography," *Phys. Rev. Lett.*, vol. 85, no. 6, pp. 1330–1333, Aug. 2000.

[126] N. Lütkenhaus, "Security against individual attacks for realistic quantum key distribution," *Phys. Rev. A*, vol. 61, no. 5, Apr. 2000, Art. no. 52304.

[127] N. Lütkenhaus and M. Jahma, "Quantum key distribution with realistic states: Photon-number statistics in the photon-number splitting attack," *New J. Phys.*, vol. 4, no. 1, p. 44, Jul. 2002.

[128] W.-Y. Hwang, "Quantum key distribution with high loss: Toward global secure communication," *Phys. Rev. Lett.*, vol. 91, no. 5, Aug. 2003, Art. no. 57901.

[129] X.-B. Wang, "Beating the photon-number-splitting attack in practical quantum cryptography," *Phys. Rev. Lett.*, vol. 94, no. 23, Jun. 2005, Art. no. 230503.

[130] H.-K. Lo, X. Ma, and K. Chen, "Decoy state quantum key distribution," *Phys. Rev. Lett.*, vol. 94, no. 23, Jun. 2005, Art. no. 230504.

[131] X. Ma, B. Qi, Y. Zhao, and H.-K. Lo, "Practical decoy state for quantum key distribution," *Phys. Rev. A*, vol. 72, no. 1, Jul. 2005, Art. no. 12326.

[132] Q. Wang, X.-B. Wang, and G.-C. Guo, "Practical decoy-state method in quantum key distribution with a heralded single-photon source," *Phys. Rev. A*, vol. 75, no. 1, Jan. 2007, Art. no. 12312.

[133] H. M. Srivastava and J. P. Singhal, "Some extensions of the Mehler formula," *Proc. Amer. Math. Soc.*, vol. 31, no. 1, pp. 135–141, Jan. 1972.

[134] R. Loudon and P. Knight, "Squeezed light," *J. Modern Opt.*, vol. 34, nos. 6–7, pp. 709–759, Mar. 1987.

[135] G. Dattoli, A. Torre, and M. Carpanese, "Operational rules and arbitrary order Hermite generating functions," *J. Math. Anal. Appl.*, vol. 227, no. 1, pp. 98–111, Nov. 1998.

Andrea Giani (Student Member, IEEE) received the Laurea degree (*summa cum laude*) in Engineering of Electronics for ICT in 2021 from the University of Ferrara, Italy. He is currently pursuing the Ph.D. degree with the Wireless Communication and Localization Networks Laboratory (WCLN Lab), University of Ferrara, Italy, which he has been a member of since 2019.

He is currently a Visiting Student with the Wireless Information and Network Sciences Laboratory (WINS Lab) at the Massachusetts Institute of Technology (MIT), Cambridge, MA, USA. His research interests include quantum information science and stochastic networks.

Mr. Giani serves as a reviewer for various IEEE journals and international conferences.

Moe Z. Win (Fellow, IEEE) is the Robert R. Taylor Professor at the Massachusetts Institute of Technology (MIT) and the founding director of the Quantum neXus Laboratory (QX Lab). Prior to joining MIT, he was with AT&T Research Laboratories and with the NASA Jet Propulsion Laboratory.

His research encompasses fundamental theories, algorithm design, and network experimentation for a broad range of real-world problems. His current research topics include ultra-wideband systems, network localization and navigation, network interference exploitation, and quantum information science. He has served the IEEE Communications Society as an elected Member-at-Large on the Board of Governors, as elected Chair of the Radio Communications Committee, and as an IEEE Distinguished Lecturer. Over the last two decades, he held various editorial positions for IEEE journals and organized numerous international conferences. He has served on the SIAM Diversity Advisory Committee.

Dr. Win is an elected Fellow of the AAAS, the EURASIP, the IEEE, and the IET. He was honored with two IEEE Technical Field Awards: the IEEE Kiyo Tomiyasu Award (2011) and the IEEE Eric E. Sumner Award (2006, jointly with R. A. Scholtz). His publications, co-authored with students and colleagues, have received several awards. Other recognitions include the MIT Frank E. Perkins Award (2024), the MIT Everett Moore Baker Award (2022), the IEEE Vehicular Technology Society James Evans Avant Garde Award (2022), the IEEE Communications Society Edwin H. Armstrong Achievement Award (2016), the Cristoforo Colombo International Prize for Communications (2013), the Copernicus Fellowship (2011) and the *Laurea Honoris Causa* (2008) from the Università degli Studi di Ferrara, and the U.S. Presidential Early Career Award for Scientists and Engineers (2004).

Andrea Conti (Fellow, IEEE) is a Professor and founding director of the Wireless Communication and Localization Networks Laboratory at the University of Ferrara, Italy. Prior to joining the University of Ferrara, he was with CNIT and with IEIIT-CNR.

In Summer 2001, he was with the Wireless Systems Research Department at AT&T Research Laboratories. Since 2003, he has been a frequent visitor to the Wireless Information and Network Sciences Laboratory at the Massachusetts Institute of Technology, where he presently holds the Research Affiliate appointment. His research interests involve theory and experimentation of wireless communication and localization systems. His current research topics include network localization and navigation, distributed sensing, adaptive diversity communications, and quantum information science.

Dr. Conti has served as editor for IEEE journals and chaired international conferences. He was elected Chair of the IEEE Communications Society's Radio Communications Technical Committee and is Co-founder of the IEEE Quantum Communications & Information Technology Emerging Technical Subcommittee. He received the HTE Puskás Tivadar Medal, the IEEE Communications Society's Fred W. Ellersick Prize, and the IEEE Communications Society's Stephen O. Rice Prize in the field of Communications Theory. He is an elected Fellow of the IEEE and of the IET, and a member of Sigma Xi. He has been selected as an IEEE Distinguished Lecturer.

Open Access funding provided by 'Università degli Studi di Ferrara' within the CRUI CARE Agreement.